A method for developing stress-strain relationships using Nanoindentations

Master Thesis, MMTM01

LUND UNIVERSITY

Fanny Linander, Ludvig Lindsjö

In collaboration with BorgWarner and the
Division of Production and Materials Engineering

Supervisors:
LTH - Jingming Zhou, Johan Persson
BorgWarner - Henrik Nilsson, Johan Flink

11 - 12 - 2020

CODEN:LUTMDN/(TMMV-5308)/1-71/2021

Supervisors:
Professor Jinming Zhou at Production and Materials Engineering
Research engineer Johan Persson at Production and Materials Engineering

Examiner:
Associate professor Fredrik Schultheiss

Industrial Supervisors:
Henrik Nilsson at BorgWarner Landskrona
Johan Flink at BorgWarner Landskrona

Authors:
Ludvig Lindsjö, Fanny Linander
Lund, Sweden 2020

Faculty of Engineering, Lund University
Box 118
SE-221 00 Lund
Sweden
Printed in Sweden
Media-Tryck
Lund University

Abstract

This thesis is a material science research collaboration between the Division of Production and Materials Engineering at Lund Faculty of Engineering and the Computer-Aided Engineerings group at BorgWarner, Landskrona. The objective of the thesis is to explore the convertion of nanoindentation load-depth curves into tensile stress-strain curves, and to provide BorgWarner Landskrona with nanoindentation data on materials used in their standard production. The materials used in the thesis includes unhardened and hardened steels as well as aluminium.

The conversion of experimental deformation data from nanoindentation in the materials into stress-strain parameters is made analytically based on well established common practice indentation theory. The direct results of extracting yield strength and strain hardening exponent of the materials were deemed to be inconclusive due to experimental effects, while a comparison between hardened and unhardened regions and different materials was possible.

Tensile tests of a C45 steel provided by the Division of Production and Materials Engineering where executed and used as reference material to confirm the validity of the analytical method. Scanning Electron Microscopy (SEM) was used to confirm the radius of the chosen indenter, a spherical indenter with a radius of 25 µm. Nanoindentation tests were performed with Nanotest Vantage from MicroMaterials for all nanoindentations. Simulations of nanoindentations were made in ANSYS Workbench 2020 R1 and used to compare both simulation with experimental load-depth curves as well as stress-strain conversion results.

Further recommendations are made to BorgWarner to execute in order to make use of the potential application of nanoindentation to extract stress-strain data from unknown materials.

Dedication

We would like to thank our family and friends and for our separate parts,

Fanny - to my father who is always in my thoughts. To my mom and beloved friends Tone, Malin, Daniel, Sebastian, Souroush, Martin, Akiko, Tilda, Hampus, Ingrid, Johannes, Jonas and Angi for your endless encouragement.

Ludvig - to my family and friends, especially Magnus, Karin, Lars and Barbro for your support throughout my education.

Acknowledgements

This thesis has been written in collaboration with BorgWarner and the Department of Production and Materials Engineering in the midst of the COVID-19 pandemic.

We want to thank Johan Persson and Jinming Zhou, our supervisors at Lund Faculty of Engineering, for sharing your knowledge with us. For always being generous with your time and helping us stay on track.

We want to thank our supervisors Henrik Nilsson and Johan Flink at BorgWarner for your continuous support and input, providing us with valuable outside perspectives of this very specific field of research.

A warm thank you to everyone at the Division of Production and Materials Engineering who have helped and supported us, including Aylin Ahadi, Dmytro Orlov, Filip Lenrick, Rebecka Lindvall and Ryszard Wierzbicki.

Thank you, Jonas Engqvist at the Division of Solid Mechanics for helping us with tensile testing, and Elin Anna Topp at the Department of Computer Science for discussing the potential of the use of machine learning in the project.

Last, but not least, we want to thank everyone at BorgWarner who have helped and supported us along the way, including Ann-Lois Nilsson, David Johansson and Leif Nordqvist.

Nomenclature

α	Constraint factor linking load and depth from an indentation to stress and strain
β	Constraint factor linking load and depth from an indentation to stress and strain
σ_y	The yield strength of a material
n	The strain hardening exponent of a material
ϵ	Strain
σ	Stress
a_c	Contact depth radius of indentation
E_i	Young's modulus of indenter material
E_m	Young's modulus of material
E_r	Reduced Young's modulus
L	Indentation load
E	Young's modulus
FEM	Finite Element Method
h_c	Contact depth of indentation
H	Hardness of material
h	Depth of indentation from original surface
Load-depth curve	Output from an indentation consisting of data points showing the force in relation to the depth
MFNN	Multi-Fidelity Neural Network
NN	Neural Network
R	Indenter radius
SEM	Scanning Electron Microscopy
S	Stiffness of material

Contents

List of Figures

List of Tables

1. Introduction

This chapter is an introduction to the thesis. It includes a brief description of BorgWarner as well as a description of the problem. The objective and goals of the thesis are presented together with limitations and target groups.

1.1 Background

The thesis is a collaboration between the Division of Production and Material Engineering, IPROD at the Faculty of Engineering of Lund University, LTH, and the Computer-Aided Engineering (CAE) group at BorgWarner, Landskrona.

1.1.1 BorgWarner Inc.

BorgWarner Inc. is an American manufacturing company operative in the automotive industry since 1880. BorgWarner have historically been most known for their transmission and all wheel drive systems and are currently producing powertrain solutions for electric, hybrid and combustion cars. Their products include electric motors and transmissions for electric vehicles, complete electrical architectures for hybrid vehicles as well as all wheel drives and transmission systems for combustion vehicles.

When developing new driveline systems, a key aspect is to increase the energy efficiency and reduce carbon dioxide emissions from the final vehicles. BorgWarner therefore prioritise the streamlining of material models for common materials, in this case hardened steels and aluminium which are commonly used in production. Efficient material models are the basis for further optimised components and thus an improved fuel economy in the final car.

CAE Group

The CAE group is a part of the Driveline Engineering Group within BorgWarner. The group was formed in 2015 and are responsible for all calculations regarding transmissions in Landskrona.

1.1.2 Nanoindentation

The field of contact mechanics studies the deformation of two solid bodies when in contact. It is a division of mechanical engineering developed by Heinrich Hertz in the late 19th century with the publication of *On the contact of elastic solids* (Hertz 1882). Simple indentation is used to study the local contact stress developed

in the contact area of a solid indenter, usually a diamond tip, and a solid piece of material in order to study its local mechanical properties. The technique was created for hardness measurements of small volumes in the mid 1950's and uses a solid indenter with known properties to penetrate the material with unknown properties. New more advanced sensors and actuators being developed made way for submicron indentation, called nanoindentation, which constantly measures the load and depth of the indentation (Schuh 2006). The result is a load-depth curve which can be used to analytically calculate several material properties such as hardness and Young's modulus. The shape of the indenter varies but the simple geometries defines the indentation contact area used in calculations of material properties. The most common types of indenters are pyramids with three (Berkovich) or four (Vickers) sides, cube corners, cones and spheres.

Most scientific progress has been made after Oliver and Pharr (1992) introduced their method for determining the contact depth. Their progress has led to better measurements of hardness and Young's modulus of an indented material. Their progress, in combination with superior finite element software and increasing capacity of computational power, has led to a large number of methods being developed for estimation of material properties based on nanoindentations. The main advantage with extracting material properties from nanoindentation data is the possibility to estimate local material properties in a way that might not otherwise be possible. For instance to determine the stress-strain relationship in a thin coating (Bouzakis, Michailidis, and Erkens 2001), or in order to determine the variations of the stress-strain relationship around a friction welded zone (Iracheta, Bennett, and Sun 2016), both of which would be difficult to estimate using a macroscale tensile test.

1.2 Problem Description

The thesis examines the potential of the use of nanoindentation on steels and aluminium used in production for certain components at BorgWarner to determine the stress-strain relationship of the materials. Using nanoindentation to determine the characteristics of the components gives a highly local image of its properties, making the method potentially useful for examining the change of properties due to heat treatment resulting in a non-homogeneous material. The thesis will include both untreated and heat treated steel as well as a standard aluminium alloy.

There are several different methods currently being used within the field on nanoindentation to determine the stress-strain relationship of a material. The thesis examines the potential of implementing some of these methods on materials provided by BorgWarner. The potential of the method to determine stress-strain relationships for heat treated material will determine which method will be chosen for further development. The goal being implementation of a regularly used and current technique within research for use in the industry.

To be able to implement a method for converting indentation data into stress-strain data, an understanding of the behaviour of a material on a nanoscale is required. It includes taking microstructural phenomenons into account in order to upscale the local imagery of nanoindentation and its three dimensional compressive forces into macroscale uniaxial tensile load (De Bono 2017).

1.3 Objective

The goal of the thesis is to provide BorgWarner with knowledge and competence concerning the potential of using nanoindentation to determine stress-strain relationships. The project aims to deliver a functioning and accessible method to directly convert indentation data from the materials provided by BorgWarner into stress-strain curves. It also aims to be able to analyse the variation of stress-strain relationship in heat treated components depending on the radial distance from the surface.

The method will be developed with the help of a reference material provided by the Division of Production and Materials Engineering, Lund Faculty of Engineering. The properties of the reference material will be determined with multiple tensile tests and used for verification of the method.

In order to provide knowledge to BorgWarner concerning the subject of contact mechanics, indentation data from the supplied materials from components in production within the company will be provided for further studies.

Goals

- Deliver a method for stress-strain conversion in an accessible and easy to use form
- Provide information on variation of stress-strain relationships in heat treated steel
- Examine if the chosen method is suitable to use with other metals such as the provided aluminium
- Provide BorgWarner with indentation data from the tested materials for further studies

1.4 Limitations

The goal of the thesis is to explore the potential of using nanoindentation to determine stress-strain relationships of a material. Nanoindentation is a large field of research with many potential methods of extracting the stress-strain curve from indentation data. The thesis will focus on determining whether one of these methods is suitable for usage in the automotive industry, and to implement that method. Focus will also be on providing the company with indentation data from the two steels and the aluminum. Other methods will be studied briefly and discussed in part to explain the motivation for choosing the particular method around which the thesis will revolve.

Although microstructural influences are an important part of the analysis of nanoindentations because of a materials inherent microstructural heterogeneity, the impact of those effects will be discussed but are not the main focus of the thesis. The analysis of experimental data is approached through the chosen method with some analytical compensation for microstructural phenomenon, but with the specific implementation of the method being of main focus.

Subjects which will be discussed but not thoroughly analysed are:

- Microstructural influences
- Indentation size effect
- Surface finish on the samples
- Influence of friction

1.5 Disposition

Methodology This chapter provides the necessary information about the methodology used in the thesis. The methodology is to support the aim of gaining knowledge on the distinct problem.

Theory This chapter accounts for the literature study and includes basic nanoindentation theory as well as a thorough theoretical base of the chosen method. The chapter accounts for theory concerning simulation of nanoindentation with finite element method. Lastly, it also includes minor theory on microstructural influences and factors determining the individual load-depth curves of an indentation.

Experimental procedure This chapter describes the procedures used for all experiments and the data handling. This includes the procedures for tensile testing, SEM, FEM simulations, nanoindentations and Python scripts.

Results This chapter concerns the experimental results. Firstly, the results of the tensile testing are presented after which the results from the the SEM of the indenter, followed by the results from the simulation of nanoindentation with finite element method. Lastly the results from the reference material and the by BorgWarner provided material is presented.

Discussion This chapter discusses the experimental results of the tensile testing, experimental results from indentation of the reference material and the provided material from BorgWarner as well as the results from simulated indentations done with finite element method. It includes experimental as well as conceptual conclusions and a larger chapter on recommendations for further work.

1.6 Target Group

The thesis aims to bridge academic research with implementation of theory in industry. The industry regards the automotive industry through BorgWarner but is of interest for all industry application of material science concerning stress-strain relationships for standard and non-standard metal used for production. Within academic research the thesis is founded in material science and the prospects of using contact mechanics to explain material properties.

1.7 Confidentiality

A confidentiality agreement has been signed with BorgWarner including disclosure of company trade secrets as well as giving BorgWarner unrestricted ownership of delivered products. Components provided by BorgWarner are to be considered company secrets and will not be discussed in detail in this thesis. Concerning the provided materials, the discussions will include necessary information to further develop on the ideas of implementing nanoindentation to determine mechanical properties of the materials but will refrain from unnecessary particulars.

2. Methodology

This chapter provides the necessary information about the methodology used in the thesis. The methodology is to support the aim of gaining knowledge on the distinct problem.

2.1 Research approach

The research covers several aspects of nanoindentation beginning with an exploratory research of the field in a literature study. It also includes an explanatory research aiming to study the cause and effect relationship through a systematic experimental design. Analysing the results of the experimental design the thesis then move to an iterative process with the purpose of improving research.

2.2 Methods

The thesis uses different experimental methods to be able to confirm the chosen analytical model of conversion, as well as for further data collection as a part of the objective.

2.2.1 Tensile tests

The properties of the reference material is extracted from experimental tensile tests made in the lab of Solid Mechanics at the Faculty of Engineering, Lund University. Six standardized tensile tests were made with a C45 steel taken from the same rod of material as the material samples used for nanoindentations of reference material.

2.2.2 Finite Element Method

The validity of method is then confirmed through finite element method simulations of a nanoindentation of the reference material.

The same procedure is then executed with experiments of nanoindentation in the empirical material taken from the same source of material sample as was used for tensile testing. Further experiments are made in different materials including unhardened and hardened steel and an aluminium alloy.

2.2.3 Scanning Electron Microscopy

To confirm the shape and condition of the used indenter, a scanning electron microscopy (SEM) evaluation was made of the indenter.

2.3 Collection of data

The objective of the thesis is a qualitative research concerning the possibility to translate experimental data into stress-strain curves. To be able to reach this objective the data collection of the tensile testing is combined and fitted to a Hollomon curve. When processing load-depth curves from experimental indentation a single indentation is not considered as valid basis of conclusion, whereby an average load-depth curve from several indentations forming a grid in the material are used for the final conversion into stress-strain curves.

3. Theory

This chapter accounts for the literature study and includes basic nanoindentation theory as well as a thorough theoretical base of the chosen method. It also includes minor theory on microstructural influences and factors determining the individual load-depth curve of an indentation.

3.1 Introductory theory

In order to be able to thoroughly analyse the potential deviation of results concerning stress-strain data converted from nanoindenation, an introductory study of common practice theory in the field is made.

3.1.1 Solid mechanics background

One of the foundations of solid mechanics is material modelling. The standard procedure for extracting the material properties is through tensile testing from which an engineering stress-strain curve is extracted. During a tensile test, a sample with known cross-section area is pulled at a constant strain rate. The engineering stress and strain are then calculated with the following equations,

$$\sigma_e = \frac{F}{A_0} \tag{3.1}$$

$$\epsilon_e = \frac{l - l_0}{l_0} \tag{3.2}$$

Where F is the force, A_0 is the original area, l is the length of the specimen and l_0 is the initial length of the specimen. These equations do not take the change in cross-section area into account and thereby do not represent the true stress and strain of the material. The engineering stress and strain are therefore converted with Equations 3.3 and 3.4.

$$\epsilon_{true} = ln(1 + \epsilon_e) \tag{3.3}$$

$$\sigma_{true} = \sigma_e(1 + \epsilon_e) \tag{3.4}$$

It is important to note that the conversion is only valid up to the ultimate tensile strength which is the highest stress in the engineering stress-strain curve. The ultimate tensile strength correlates to when necking begins in the tested specimen and the area starts to rapidly decrease, and the engineering stress decreases. The difference between the two curves can be seen in Figure 3.1

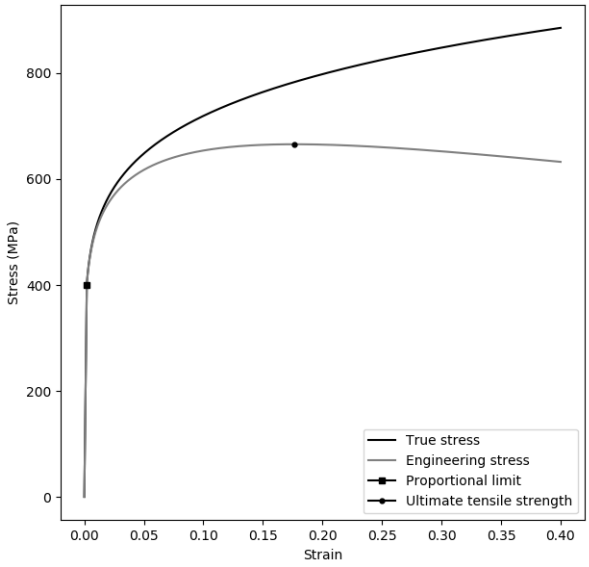

Figure 3.1: Schematic figure showing the difference between engineering stress and true stress and the proportional limit and ultimate tensile strength

From the true stress-strain curve, it is possible to extract material parameters such as Young's modulus (E), yield strength (σ_y)and strain hardening exponent (n). Many different material models exist and are suitable for different materials. One of the most common models for metals is the plasticity model proposed by Hollomon (1945) with the following equation

$$\begin{cases} \sigma = E\epsilon \text{ if } \sigma < \sigma_y \\ \sigma = K\epsilon^n \text{ if } \sigma \leq \sigma_y \end{cases} \tag{3.5}$$

In order to achieve continuity, the constant K in 3.5 can be replaced with 3.6.

$$K = \sigma_y \left(\frac{E}{\sigma_y} \right)^n \tag{3.6}$$

Depending on context, the yield strength can be defined in different ways. When applying the Hollomon relationship in 3.5, the yield strength is defined as the proportionate limit with 0% plastic strain. In case the material does not exhibit a clear yield strength, it is commonly defined as the stress corresponding to 0.2% plastic strain. When comparing these two definitions of yield strength, the one defined by the proportional limit will always generate a lower value.

3.1.2 Hertz' law of contact

In the 1880s, Heinrich Hertz laid the foundation for the field of contact mechanics. He researched how two elastic bodies in contact behave. From his works (Hertz 1882) Equation 3.7 can be derived.

$$h_e = \frac{1}{2} \left(\frac{3L}{4E_r} \right)^{2/3} \left(\frac{1}{R} \right)^{1/3} \tag{3.7}$$

Where h_e is the elastic contact depth, L is the applied load, E_r is the reduced modulus according to Equation 3.8 below, and R is the indenter radius.

$$\frac{1}{E_r} = \frac{1-\nu_m^2}{E_m} + \frac{1-\nu_i^2}{E_i} \tag{3.8}$$

where E_m and ν_m are the Young's modulus and Poisson's ratio of the indented material while E_i and ν_i are the Young's modulus and Poisson's ratio of the indenter.

3.1.3 Nanoindentation

One of the most important estimations for analysing nanoindentations is the contact depth. The contact depth is needed for most common applications of nanoindentations, among others are measurement of the hardness (H) and Young's modulus (E), and estimations of the stress-strain curve of the material. One of the most common methods used today is Equation 3.9 proposed in its final form by Oliver and Pharr (1992).

$$h_c = h - \epsilon\frac{L}{S} \tag{3.9}$$

h_c is the contact depth, h is the total depth, ϵ is a constant depending on the indenter geometry, P is the load and S is the contact stiffness which represented by the slope of the unloading curve at the onset of unloading, commonly written as follows:

$$S = \left[\frac{dL}{dh}\right]_{h_{max}} \tag{3.10}$$

In the same article (Oliver and Pharr 1992), it is proposed to use a power law, Equation 3.11, in order to represent the unloading curve, instead of the linear approximation which had been used earlier.

$$L = a(h - h_f)^m \tag{3.11}$$

In Equation 3.11, a, h_f and m are fitting parameters which are found by least squares fitting procedure. From the values for the maximum contact depth it is possible to evaluate the reduced modulus and hardness according to Equations 3.12 and 3.13.

$$E_r = \frac{\sqrt{\pi}}{2\beta}\frac{S}{A(h_{c,max})} \tag{3.12}$$

$$H = \frac{L_{max}}{A(h_{c,max})} \tag{3.13}$$

The major drawback of this method for finding the contact depth, is its dependency of the unloading curve. A new technique called Continuous Stiffness Measurement (CSM) has therefore been introduced. It is a experimental procedure where the nanoindentation machine applies the increasing load with periodical unloads from which the stiffness can be measured. From the CSM protocol, it is therefore possible to extract the contact stiffness from several points along the load-depth curve.

3.1.4 Microstructure

As mentioned, microstructural influences has not been a main focus of this thesis, but in the following section some microstructural phenomena are mentioned as well as how they are taken into account during the analysis of the experimental data. When extracting the mechanical properties of the materials, only selecting one experimental indentation to describe the stress-strain relationship would become biased because of a materials microstructural heterogeneity. Instead, a grid of indentations are used to produce an average load-depth curve. The average is intended to better describe the total effect of the different microstructural influences on surface response. However, microstructural phenomenons of materials are discussed as a potential source of error in experimental implementation. It is used to understand the complexity of the influences it has on the results of the specific technique of deformation in compression on such a scale as nanoindentation. When probing material on a nanoscale it could be comparable in size to grain size and dislocations, thus compromising the assumption of working on a continuum.

Microstructure of C45 steel

The sample collected from LTH and subsequentially used as a reference material for the thesis is used for tensile tests showing a clear yield strength of 430 MPa in accordance with the corresponding data sheet for C45 from Saarstahl. Looking at the specifics of this material, a C45 steel, it means that it would be heat treated by quenching and tempering. The microstructure of C45 steel heavily depends on the manner of which it has been heat treated, depending on temperature as well as quenching media. The microstructure of the material sample is analysed by using the microscopes, Figure 3.2, of the nanoindenter and deamed to be pearlitic with graphite flakes (Blaoui, Zemri, and Abdessamad 2018). To avoid relating material stress-strain properties to microstructurally unbalanced indentations, grids are set up to be used in the confirmation of the method through the C45 as a reference material.

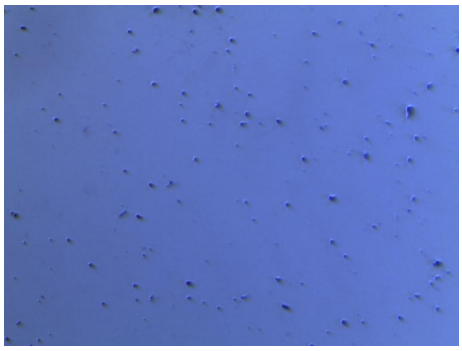

Figure 3.2: Image of the microstructure of the C45 reference material.

Deformation mechanisms

Equation 3.9 as proposed by Oliver and Pharr (1992), a calculation of contact depth where the effects of sink-in is based on Sneddon's force-displacement relationship for conical indenters (Sneddon 1965). That is, a certain consideration has been taken

into account where the material sinks inwards when deformed with the indenter because of its elastic behaviour. However, because of plastic deformation the material can also instead pile up around the indenter (De Bono et al. 2017). Both phenomena means that the calculation of contact area, a key calculation for the mean pressure of indentation, becomes compromised when it is not taken into account. The phenomenon sink-in and pile-up can be seen in Figure 3.3. In the formulating of the maximum depth of penetration taken from (Sneddon 1965),

$$h_{max} = h_c + h_a \tag{3.14}$$

Sneddon suggests that the force-displacement relationship for conical indentation can be described as follows,

$$h_a = \varepsilon \frac{L}{S} \tag{3.15}$$

Where ε is an indenter dependant constant, being 0.75 for spherical indenters. The relationship creates the defined equation for contact depth,

$$h_c = h - \varepsilon \frac{L}{S} \tag{3.16}$$

Pileup and sink-in can thereby have a large effect on the final result of converting load-depth curves of an indentation into mechanical properties.

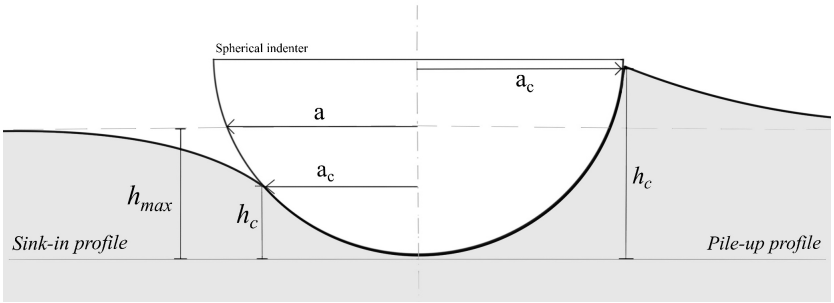

Figure 3.3: Pileup and sink-in during an indentation

Indentation size effect

One common phenomena that might occur in nanoindentation experiments, is the Indentation Size Effect (ISE) which causes a material to exhibit a higher hardness at smaller depth. Pharr, Herbert, and Gao (2010) performed extensive research in order to describe the phenomena. Their modelling was based on the model developed by Nix and Gao (1998). According to the Nix and Gao (1998) model, a material appears to have a higher hardness at smaller depths due to a deficiency of geometrically needed dislocations. These dislocations are needed in order to enable the material flow due to the material displaced by the indenter.

For pyramidical and conical indenters, the ISE is most prominent down to the depth of approximately 1 µm. In the case of spherical indenters, the depth is not the regulating factor, instead the indenter radius appears to be the factor determining whether the ISE occurs or not. According to Pharr, Herbert, and Gao (2010), the ISE will be most prominent for radii smaller than 100 µm.

3.1.5 Finite Element Method

The finite element method is a commonly used approach for calculating stresses, strains, displacements etc. in a given scenario. Instead of calculating forces and displacements by performing integrals over the whole body, the method works by dividing the model into small, finite elements which are then used for the calculations with a certain degree of approximations.

In order to decrease the complexity of the finite element analysis of a nanoindentation, several simplifications are possible. Instead of performing a full 3D-analysis, it is possible to perform the analysis on a symmetric half model (Iracheta, Bennett, and Sun 2016), one sixth of a three-sided Berkovich indenter (Haj-Ali et al. 2008) or simply as a 2D axisymmetrical model (Beghini, Bertini, and Fontanari 2006). The 2D model is especially accurate in the case of axisymmetrical indenters, such as spheres, but research has been made on using a 2D cone with a 70.3° half-angle as an approximation of a Berkovich or Vickers indenter in 2D (Min et al. 2004). This approximation has been used with good results by several researchers, including De Bono et al. (2017), Khan et al. (2010) and Bouzakis, Michailidis, and Erkens (2001).

The effects of friction and the stiffness of the indenter are also common topics of discussion. Xu and Chen (2010) use spherical diamond indenters and assume that the indenters are rigid in comparison to the indented materials, while Beghini, Bertini, and Fontanari (2006) come to the conclusion that their spherical tungsten-carbide indenter should be assumed to be elastic. Xu and Chen (2010) also examine the effect of friction on the spherical indentation process. Their results were a variation at most 17% between frictionless contact, and a friction coefficient of 0.5. The largest difference occurred at relatively large depth and when the ratio between the Young's modulus and yield strength (E/σ_y) was relatively large and the strain hardening exponent (n) was small. The depths where the friction influenced their results, the method proposed by Xu and Chen (2010) correlated to approximately 10% strain. Xu and Chen (2010) decided to use 0.1 as the friction coefficient, which is in line with the works by Chung et al. (2009) used 0.11 and Taljat, Zacharia, and Kosel (1998) who used 0.2. In contrast, when performing simulations of pyramidical indentations, the friction is usually assumed to be zero due to its small contribution of the load-depth curve (De Bono et al. 2017; Iracheta, Bennett, and Sun 2016; Khan et al. 2010).

3.2 Considered methods

3.2.1 Brute FEM

One common method to acquire the uni-axial data from a indentation experiment, is modelling it in a FEM with varying tensile data, yield strength and strain hardening coefficient. The number of required iterations can be as low as between ten and twenty in the study by Iracheta, Bennett, and Sun (2016). The method is very simple and works on a large variety of materials. However, every experiment requires a complete iterative process and will thereby be very computationally heavy since every new indentation will require several iterations in order to evaluate the new material data, such as the gradient in the hardened steel.

In order to extract the material properties, several methods are available with

varying degrees of efficiency. Bouzakis, Michailidis, and Erkens (2001) proposed a method where the stress-strain curve is piecewise estimated through FEA:s. The method was then further developed by Valiev et al. (2007) and Jeong et al. (2014). This approach simulates an indentation up to a certain amount of plastic strain where it iterates until it matches the load-depth curve and has thereby found the correct stress for that point on the stress-strain curve. The iterative procedure sets a plastic strain and performs a simulation, the simulated load-depth curve is then compared with the experimental one. If the error between the two curves is too large, the stress corresponding to the tested plastic strain in the stress-strain curve is adjusted and a new simulation is set up. If the error is smaller than the threshold, the method has found a correct value for the point on the stress-strain curve and uses it in the simulations for the following points.

Iracheta, Bennett, and Sun (2016) propose a different approach where they find a continuous material model defined by Hollomon's plasticity model. Their approach is based on an optimisation algorithm in MATLAB in combination with FEAs in ABAQUS. When a FEA has been completed, every load step is compared to the experimental indentation data and the total error between the experimental and the simulated curve is calculated. This result is then sent back to the optimisation algorithm which adjusts the Young's modulus, yield strength and strain hardening exponent which are then used to start a new simulation. This process continues until the total error is at an acceptable level. This approach required around ten iterations with 200 load steps before converging.

3.2.2 FEM database

Instead of setting up an iterative FEA based process for every single indentation, it is possible to create a large grid of load-depth curves for different combinations of material parameters as made by De Bono et al. (2017) and in De Bono (2017). They describe two different procedures for estimating the material properties. Both are based on a large number of simulated indentations with varying material parameters.

The first method can be applied either with an average load-depth curve from all indentations, or performed for every single indentation. The indentation curve is then compared to the simulated load-depth curves. The material properties of the indented material are then estimated with the parameters from the best matching curve. The choice between using the average loading curve or all curves is highly dependant on whether the load-depth curves are similar with little scatter, or if the material contains multiple phases which cause a large span of scatter. Using the average curve gives a more reliable result for the bulk material in the case with less scatter. However it might cause an unintended bias between phases if there is a large scatter or different concentrations of curves as seen in Figure 3.4.

In an attempt to counteract unintended biases, De Bono et al. (2017) suggest a new method which is also capable of providing continuous results for the material parameters instead of only the discrete points from the simulations. The approach compares every load-depth curve with every simulated curve and the extracted result is the weighted average of all simulated material parameters where the weights are based on the error between the respective simulated curve and the respective experimental curve. The method with the weighted averages from all indentations and simulations perform significantly better in accurately determining the yield

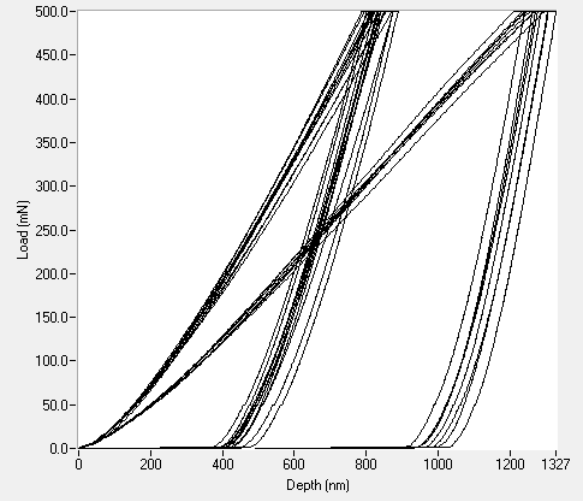

Figure 3.4: Load-depth curves with two dominant phases or regions generating different results although the experiments are made in the same sample

strength and strain hardening exponent. It is also less sensitive to the resolution of the simulated grid. It provides similar results even if the number of points is reduced.

Khan et al. (2010) also performed a reverse analysis based on a simulated grid where the closest match is assumed to be the material properties, but instead of comparing the the indentations curves directly, they compare four parameters describing the load-depth curve. The four parameters are C from the following description of the load-depth curve $L = Ch^2$, the maximum force, P_{max}, the unloading stiffness, S and the ratio between plastic and total work, W_p/W_t. Their method provided accurate results with a smaller number number of simulations, around 130 simulations, than De Bono et al. (2017) who required around 4000 simulations. Khan et al. (2010) managed to reduce the number of simulations needed by making a number of assumptions regarding the exponent and the yield strength. The yield strength was estimated from the hardness of the material and based on that yield strength they set the boundaries for the simulation grid. The grid boundaries for the strain hardening exponent were based on reference values for similar aluminium alloys.

Instead of depending on the simulated load-depth curves, Beghini, Bertini, and Fontanari (2006) suggest a method where a large number of FEAs build a database from which a function describing the link between the force and the depth is created. The method is based on the description of the load-depth curve as the following dimensionless function where L is the load, D is the diameter of the spherical indenter, h is the indentation depth and A_k represent four constants based on the material properties.

$$\frac{L}{ED^2} = \sum_{k=1}^{4} A_k * \left(\frac{h}{D}\right)^{k/2} \tag{3.17}$$

In order to relate the load-depth function to the material properties, the relationship between A_k and the proportional limit, σ_0, and strain hardening exponent, n, is described with the following equation:

$$A_k = \sum_{i=1}^{6} \sum_{j=1}^{6} \alpha_{ijk} * \sigma_0^{i-1} * n^{j-1} \tag{3.18}$$

Combining Equations 3.17 and 3.18 creates a function with 144 constants which were fitted to the results from the database with simulated indentations. In order to determine the material properties of a material from an indentation curve, an iterative process is initiated for every data point on the indentation curve. For a given data point, the depth is used to calculate a theoretical load which is compared to the correlating experimental load. The calculations begin with arbitrary values for the proportional limit and strain hardening exponent, which are then modified until the result converges.

An interesting note is that both, Beghini, Bertini, and Fontanari (2006), and De Bono et al. (2017) consider the Young's modulus as a known variable, at least by material class (Beghini, Bertini, and Fontanari 2006), or through analysis of the unloading data (De Bono et al. 2017).

3.2.3 Machine Learning Algorithms

When extracting critical properties using experimental nanoindentation the results can be inaccurate due to the nature of experimental data experiencing noise. Machine Learning is a powerful tool in order to reduce that noise and approach more accurate results with the help of modern processing power and artificial intelligence.

It combines being a modern and novel technique, with the possibility to improve the accuracy of prediction using the regularly used nanoindentation equipment. Together with the capacity of creating high amounts of synthetic data such as simulation of nanoindentation it can be a relatively cheaper way of creating the vast amount of data accumulation needed to develop artificial learning algorithms. Something that would be relatively expensive if experimental data only were to be used.

A machine learning algorithm is based on an automatic learning process and has the ability to improve with experience. The model thereby have the possibility to deliver results with the accuracy needed for material testing within industrial application.

MIT has recently (Lu et al. 2020) released a study of using Artificial Neural Networks to extract the elastoplastic properties of metals and alloys. A neural network (NN) is a computer generated set of algorithms that connects input data with output data, trying to define the relationships between the two by mimicking the neurons of a biological brain. It can be a very complicated system consisting of an almost infinite number of neurons and layers, or it can be a very simple one merely filling the gaps of uncomplicated analytical solutions to a certain problem.

Since converting load-depth curves to stress-strain curves is a translation involving many different factors of material properties and currently being without a widely accepted analytical approach, machine learning algorithms could be argued to make use of a larger amount of information available with simulations. The method is thereby commonly used in combination with a FEM-database.

Historically, existing machine learning algorithms require all data points of an individual loading curve to train the algorithm to extract the stress-strain parameters.Lu et al. (2020) instead use parameters from an analytical function fitting of

the loading, or unloading, curve, and therefore drastically reduces the processing complexity of the system. The parameters used to describe the loading curve are the loading curvature, C, initial unloading slope dP/dh and the ratio of the plastic work and the total work W_p/W_t. This description of the loading curve makes the large number of individual data points otherwise needed obsolete.

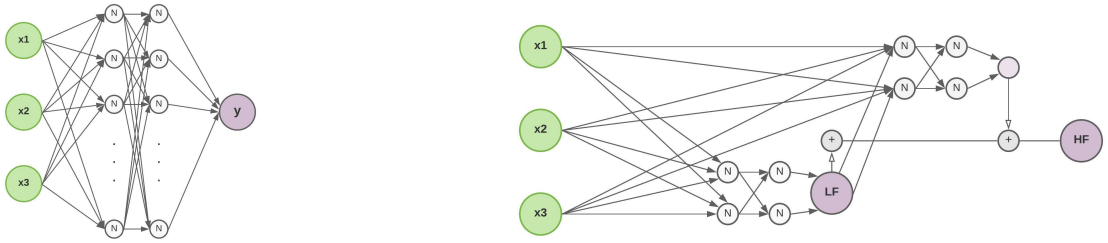

(a) Single-Fidelity Neural Network

(b) Multi-Fidelity Neural network

Figure 3.5: Visual representation of difference between Single- and Multi-Fidelity Neural Networks. a) x1-3 representing input data, N neurons and y the output data (label). b) with output data from Low Fidelity (LF) and High Fidelity (HF) data constitutes the final output HF.

The method also uses a formula for training the neural network called Multi-Fidelity Neural Network (MFNN). The difference from the regular Single-Fidelity Neural Network can be seen in Figure 3.5. Commonly, neural networks are trained with sets of data having a similar level of accuracy. But in reality, a set of lower fidelity data, meaning data having a lower level of accuracy, could be fairly inexpensive while a set of higher fidelity data can be expensive to produce. The Multi-Fidelity Neural Network combines the two, creating different levels of fidelity data for training sets to interconnected neural networks (Meng and Karniadakis 2019). In practice, this means using low fidelity data, 2D FEM simulations of nanoindentations, to train one neural network, and then interconnect this with another neural network that has been trained with high fidelity data, 3D FEM simulations and experimental nanoindentations. This reduces the required number of high fidelity data without diminishing an extensive training process. Lu et al. (2020) also introduce the hybrid training called transfer learning, where additional new experimental data on material with properties similar to those of the unknown material further trains the high fidelity subnetwork to boost the method (Lu et al. 2020).

3.2.4 Analytical approach

Most analytical approaches for determining the yield strength or stress-strain curve, are based on the works by Tabor (1951) who found connections between the stress and the mean indentation pressure. The mean indentation pressure is defined as the applied force divided by the contact area as seen in Equation 3.19 where a_c is the contact radius.

$$p_m = \frac{L}{A_c} = \frac{L}{a_c^2 \pi} \tag{3.19}$$

The conclusions made by Tabor (1951) were that the onset of plastic flow occurs when the mean contact pressure is 1.1 times larger than the yield strength,

$$p_m = 1.1\sigma_y \tag{3.20}$$

When the indentation is fully plastic, the mean pressure will be around three times larger than the stress,

$$p_m = C\sigma, C \approx 3 \tag{3.21}$$

Tabor (1951) also proposed a link between the indentation load and the representative stress, as well as between the ratio a_c/R and the representative strain, where a_c is the contact radius and R is the indenter radius.

$$\sigma_r = \frac{1}{\alpha}\frac{L}{a_c^2\pi} \tag{3.22}$$

$$\epsilon_r = \beta\frac{a_c}{R} \tag{3.23}$$

In Equations 3.22 and 3.23 α and β are constraint factors linking the measured properties to the tensile properties. As stated earlier, α is around three for most metals and β is 0.2 according to Tabor (1951). Several attempts have been made to improve the method proposed by Tabor (1951) by improving the estimation of the constraint factors. Chang et al. (2018) suggested a connection between the constraint factors where they depend on the ratio between the reduced modulus and the Young's modulus, shown in 3.24. However, it should be noted that Equation 3.24 is only valid in the transition between the elastic and plastic regions and preferably in a material with a sharp transition from elastic to plastic behaviour.

$$\alpha\beta = \frac{4}{3\pi}\frac{E_r}{E} \tag{3.24}$$

From the relationship it is possible to extract the other constrain factor as long as one of them is known. Chang et al. (2018) suggest that α is constant at 3.2 for a spherical indenter in accordance with the analytical solution from Shield (1955). Although Chang et al. (2018) got decent results in the fully plastic region, the solution is only valid if the material exhibits a sharp elastic-plastic transition and might generate large deviations in a longer elastic-plastic region.

Ahn and Kwon (2001) researched further formulations of the representative stress and strain. They concluded that the representative stress could be well described with the original formulation by Tabor (1951)with the stress constraint factor $\alpha = 3$, especially when corrections for pileup and sink-in were made. Regarding the representative strain, they tested four different definitions, each representing the strain in the material at different locations around the indentation. They found that the best fitting description, leading to best results was the following equation:

$$\epsilon_r = \beta * tan\gamma = \frac{\beta}{\sqrt{1-(a_c/R)^2}}\frac{a_c}{R} \tag{3.25}$$

In Equation 3.25, γ is the angle of contact which can be rewritten to instead include the contact radius, a_c, and the indenter radius, R.

Xu and Chen (2010) continued to develop the method from Ahn and Kwon (2001). They found Equation 3.25 to be a good approximation of the indentation

strain, but proposed a new relationship between the constrain factors as well as a new definition of the contact radius. In order to better handle the effects of pileup and sink-in, they suggested that the elastic contact depth from Hertz contact formulation in Equation 3.7 should be subtracted from the total indentation depth resulting in the following equation.

$$h_c = h - \frac{1}{2}\left(\frac{3L}{4E_r}\right)^{2/3}\left(\frac{1}{R}\right)^{1/3} \tag{3.26}$$

$$a_c = \sqrt{2h_cR - h_c^2} \tag{3.27}$$

$$a_c = \sqrt{\left(2R - h + \frac{1}{2}\left(\frac{3L}{4E_r}\right)^{2/3}\left(\frac{1}{R}\right)^{1/3}\right)\left(h - \frac{1}{2}\left(\frac{3L}{4E_r}\right)^{2/3}\left(\frac{1}{R}\right)^{1/3}\right)} \tag{3.28}$$

Equation 3.28 is the result from combining Equations 3.27 and 3.26. The advantage with this formulation, is the possibility to evaluate the contact area, based on only the load, depth, reduced modulus and indenter radius. Which is in contrast to other formulation of the contact radius where either the strain hardening exponent needs to be known, or the stiffness in every data point. Xu and Chen (2010) evaluated the equation through a great number of FEA simulations where they compared the actual contact radius to the calculated radius which they calculated using various methods, including the one proposed by Oliver and Pharr (1992). In their evaluation, Xu and Chen (2010) came to the conclusion that Equation 3.28 provides a good estimation of the contact area in comparison with the other methods.

$$\sigma_{ind} = \frac{1}{\alpha}\frac{L}{a_c^2\pi}, \tag{3.29}$$

$$\epsilon_{ind} = \frac{\beta}{\sqrt{1-(a_c/R)^2}}\frac{a_c}{R} \tag{3.30}$$

According to Xu and Chen (2010), the indentation stress-strain curve based on Equations 3.29 and 3.30 match the engineering stress-strain curve. In the engineering stress-strain curve, the increasing stress due to strain hardening is eventually surpassed by the effect of necking in the specimen. Similarly, the indentation stress-strain curve exhibits the same behavior. Although Xu and Chen (2010) did not examine the reason why it occurs, their theory is that the decrease in stress is due to geometric variations, in line with the necking phenomena.

Based on the new formulation of the contact radius and the chosen formulations of the indentation stress and strain, Equations 3.29 and 3.30, Xu and Chen (2010) proceeded to find the optimal values for α and β. Both values are highly material dependent and therefore they set up a large number of FEAs for various materials with varying strain hardening exponent, n, and ratio between Young's modulus and yield strength, E/σ_y. Their findings were that α depended mainly on the strain hardening exponent, while β depended on both the strain hardening exponent and the Young's modulus to yield strength ratio. Their results were then verified against common engineering materials with stress-strain curves from tensile tests. The verifying experiments were performed in A533 steel with an indenter with 788 µm radius, and in A2024 aluminium with a 20 µm indenter.

3.3 The chosen method

After evaluating the different available methods, it was decided to implement the analytical method proposed by Xu and Chen (2010) due to its relative simplicity and their thorough description of the method.

3.3.1 Assumptions

The implementation of the method is based on a number of assumptions which need to be clarified.

The first major assumption, is that the three dimensional compressive stresses in the material occurring during a nanoindentation can be directly linked to the tensile properties acquired through a tensile test. Most metals have a similar tensile and compressive behaviour, but certain brittle metals have a larger yield strength in compression than in tension which might lead to errors in the conversion to stress and strain.

Secondly, it is assumed that the tested materials can accurately be described by the Hollomon power law as seen below.

$$\begin{cases} \sigma = E\epsilon \text{ if } \sigma < \sigma_y \\ \sigma = K\epsilon^n \text{ if } \sigma \leq \sigma_y \end{cases} \tag{3.31}$$

where

$$K = \sigma_y \left(\frac{E}{\sigma_y}\right)^n \tag{3.32}$$

Thirdly, the indenter is assumed to have a constant radius in close proximity to its nominal value of 25 µm. This assumption is necessary in order for the conversion to be possible. This is due to Equations 3.26 and 3.30 being directly dependant on the radius being constant and would otherwise need to be reworked.

Finally, it is assumed that Equation 3.26 accurately can describe the contact depth. In order for the method to work properly, it is necessary to accurately determine the contact area even with pileup or sink-in.

3.3.2 Implementation of the method

As stated earlier, the loading curve from a spherical nanoindentation can be converted using the following equations.

$$\sigma_{ind} = \frac{1}{\alpha}\frac{L}{\pi a_c^2} \tag{3.33}$$

$$\epsilon_{ind} = \frac{\beta}{\sqrt{1-(\frac{a_c}{R})^2}}\frac{a_c}{R} \tag{3.34}$$

Where the constraint factors α and β are material dependent. Their dependency on the material parameters was examined through extensive FEM simulations by Xu and Chen (2010) and the following equations were found.

$$\alpha = q_1 + q_2 n \tag{3.35}$$

$$\beta = \frac{p_1 + p_2 n + p_3 \eta + p_4 n^2 + p_5 \eta^2 + p_6 \eta n}{1 + p_7 n + p_8 \eta} \tag{3.36}$$

where

$$\eta = ln(E/\sigma_y) \tag{3.37}$$

Xu and Chen (2010) listed all the constants needed to calculate α and β in their article and they can be seen in Table 3.1.

Coefficients for α	Value
q_1	4.30731
q_2	-2.14173
Coefficients for β	Value
p_1	-0.10484
p_2	0.65039
p_3	0.03770
p_4	0.68093
p_5	-0.00348
p_6	-0.05567
p_7	3.36158
p_8	-0.16857

Table 3.1: Coefficients used to calculate α and β

3.3.3 Forward and reverse analysis

When performing conversions from nanoindentations to stress and strain, there are two types of analyses, forward and reverse. In the forward analysis, the material parameters are known and the analysis provides a verification of the method. However, in the reverse analysis, the material properties are not known in advance and an iterative procedure needs to be applied. A flowchart of the reverse procedure can be seen in Figure 3.6.

In order to perform a reverse analysis using the method method from Xu and Chen (2010), a load-depth curve from a spherical indentation test is transformed using Equations 3.29 and 3.30. This initial curve is created using an arbitrary guess for α and β. The indentation stress-strain curve is then assumed equal to the engineering curve, meaning it is possible to convert the indentation stress and strain to true stress and strain using Equations 3.3 and 3.4. From the true stress-strain curve, it is then possible to extract a value for the yield strength and the strain hardening exponent, which in turn generates a new set of α and β which can then be used in the next iteration. This process is then repeated until the values for the yield strength and strain hardening exponent has converged.

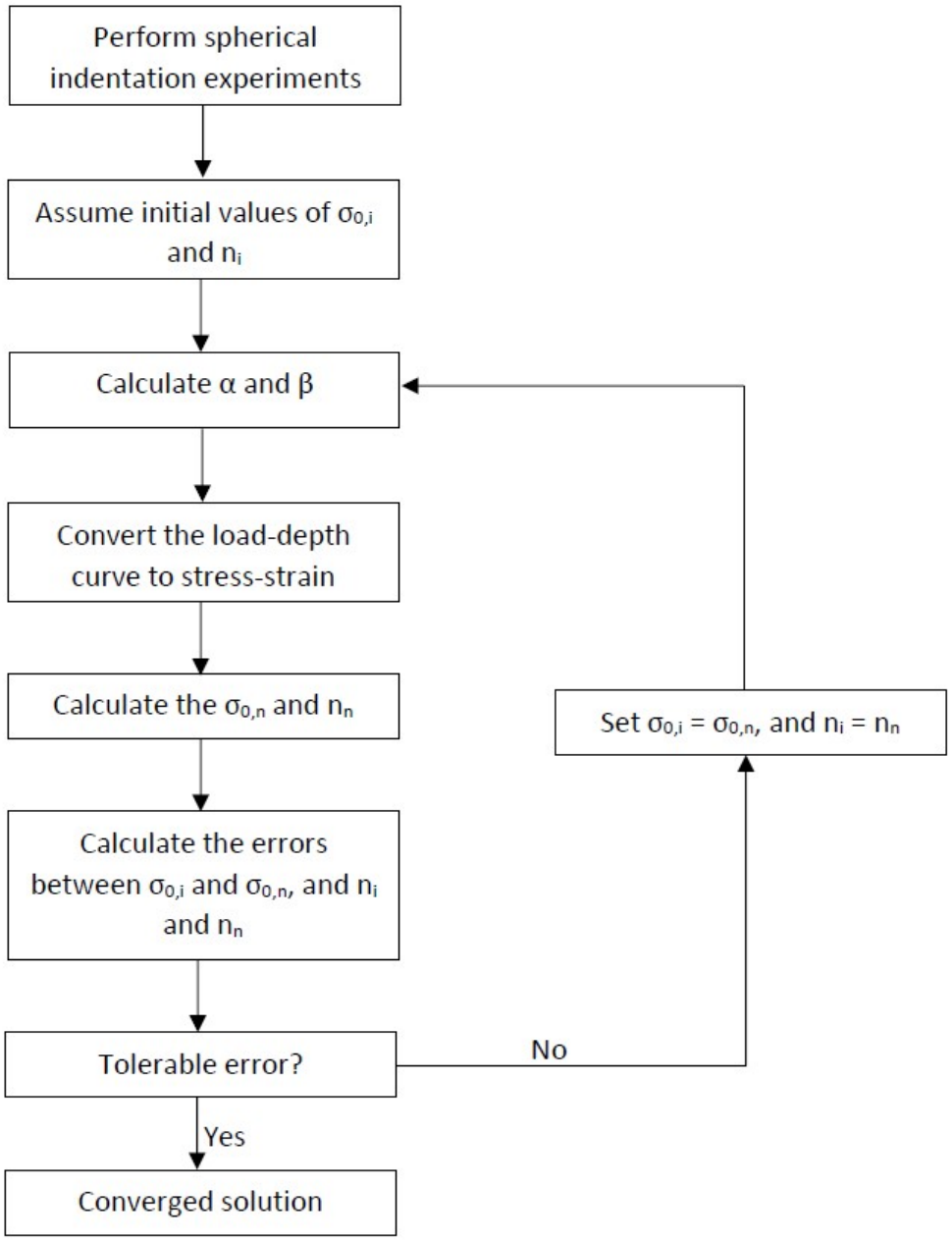

Figure 3.6: Flowchart showing the reverse procedure of the chosen method.

4. Experimental Procedures

This chapter will describe the procedures used when performing experiments and the handling of the output data.

4.1 Tensile test

4.1.1 Experimental setup

In order to perform the tensile test of the C45 reference material, six samples were prepared as seen in Figure 4.1a. They were then mounted into the testing machine with a split collar as seen in Figure 4.1b. An extensometer was then mounted onto the sample providing accurate data on the displacement, the setup in the machine can be seen in Figure 4.1c. The test was then initiated with a constant rate of displacement and the associated computer program sampled the values of the force and displacement.

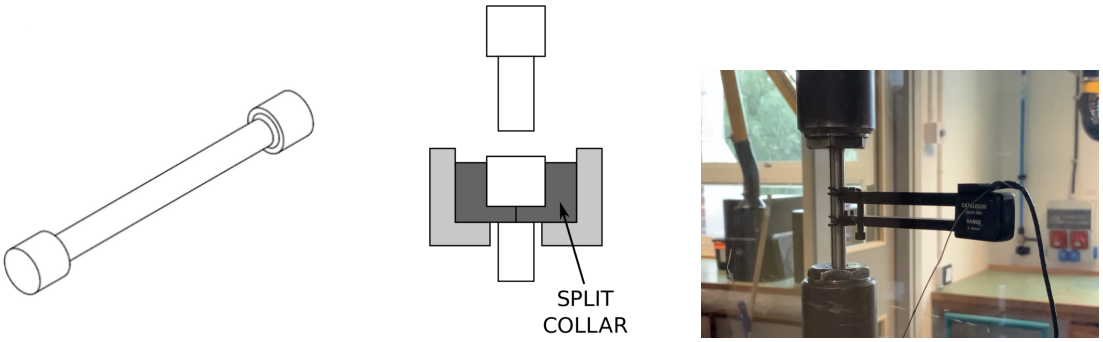

(a) CAD model of the samples for tensile testing

(b) Sample mounting for the tensile test

(c) Sample mounted in the tensile testing machine with extensometer

Figure 4.1: Model of the samples and the setup for the tensile tests

4.2 Scanning Electron Microscopy (SEM)

In an effort to evaluate the condition of the indenter, it was examined using a Scanning Electron Microscope. Due to limited options to mount the indenter in the microscope, the first setup allowed the indenter to be examined from the top and 90° from one side. In order to evaluate the indenter on all sides, the indenter was mounted in a way where it could be examined from all sides at a 60° angle.

4.3 Finite Element Method

In order to verify the method, a number of FEM simulations were set up. Based on the setups in the article by Xu and Chen (2010) two set ups were defined. One with a 20 µm indenter in aluminium A2024, and one with a 788 µm indenter in a A533-B steel. A third simulation was set up based on the data from the tensile test of the C45 and the same indenter size as used in the machine, 25 µm.

4.3.1 Experimental setup

The materials were modeled with a multilinear plasticity model in ANSYS Workbench. The material parameters were therefore used to create a large number of data points describing the stress-strain curve which were then used in the ANSYS model. The used material parameters can be seen in Table 4.1.

All simulations were setup under displacement control to a predefined indentation depth. The indenter had a Young's modulus of 1141 GPa and Poisson's ratio of 0.07. The friction coefficient was set to 0.1.

Material property	**A2024**	**A533-B**	**C45 reference**
σ_0	256 MPa	350 MPa	331 MPa
n	0.19	0.127	0.216
Young's modulus	73.1 GPa	210 GPa	180 GPa
Poisson's ratio	0.3	0.3	0.3
Indenter radius	20 µm	788 µm	25 µm
Indentation depth	5 µm	200 µm	1.35 µm

Table 4.1: Material and experimental parameters used in the FEM simulations

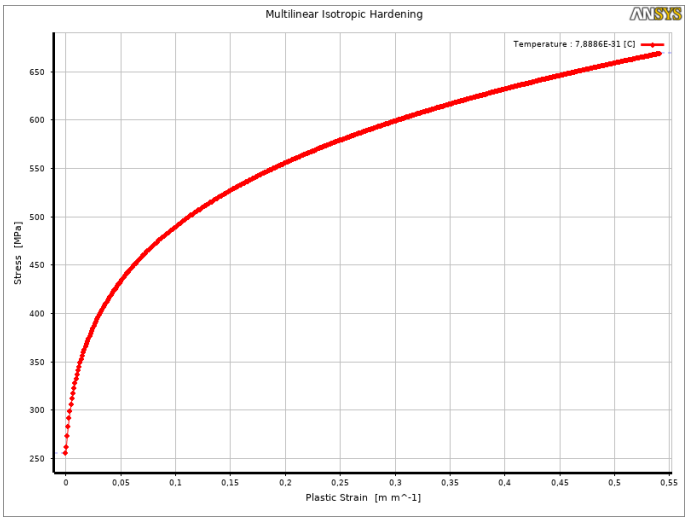

Figure 4.2: The plastic properties in FEM for the aluminium A2024 used by Xu and Chen (2010)

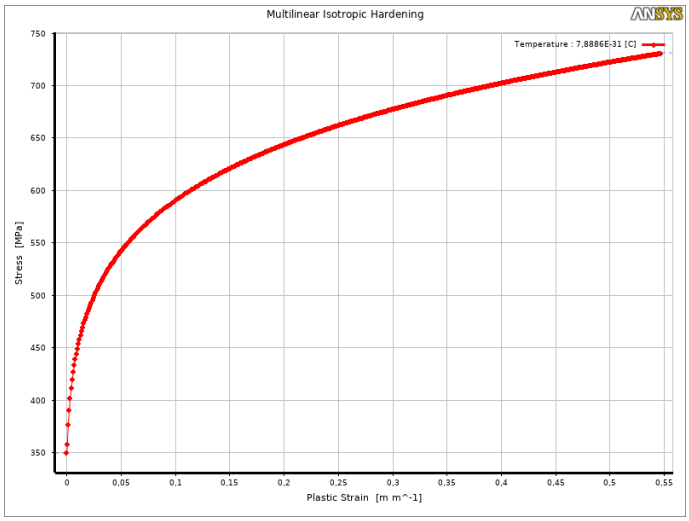

Figure 4.3: The plastic properties in FEM for the A533-B steel used by Xu and Chen (2010)

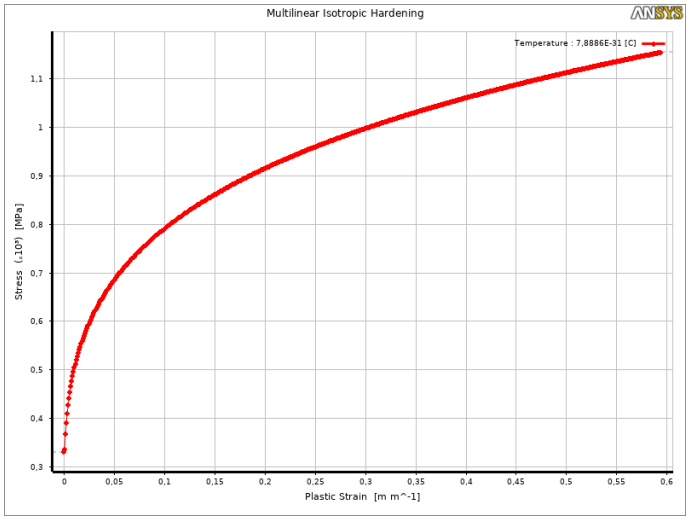

Figure 4.4: The plastic properties of the C45 reference material for FEM.

When creating the models for the indentation simulations, an axisymmetric model was chosen. Therefore the indenters were modelled as a quarter of a circle and the sample as a rectangle, as seen in Figures 4.5a to 4.6a. The size of the sample was set depending on material and indentation depth. The depths were initially set to match the indentations in the article (Xu and Chen 2010), but due to convergence issues at the larger depths in the aluminium the depth was reduced to 5 µm. The simulation in the C45 steel was made to match the depths of the experimental indentations. Since the depths in the spherical indentations are relatively small compared to the other simulations, a smaller sample model could be used for the C45 simulation.

The mesh was refined in the area around the contact where the largest deformations occurred.

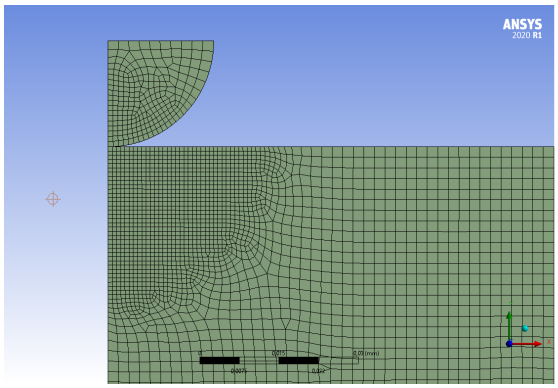

(a) The mesh used for the FEM-indentation in the aluminium from Xu and Chen (2010)

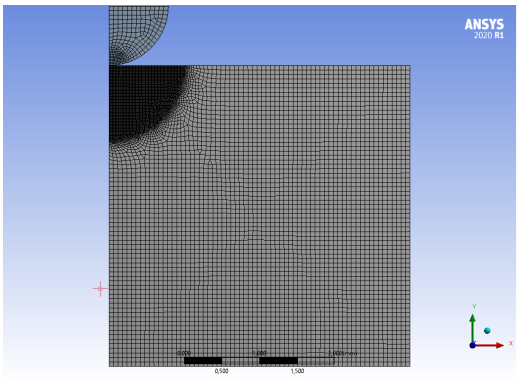

(b) The mesh used for the FEM-indentation in the steel from Xu and Chen (2010)

Figure 4.5: From ANSYS 2020 R1

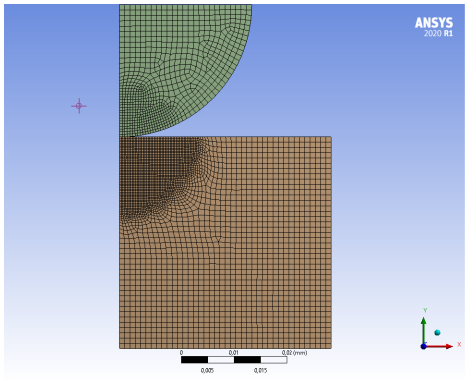

(a) The mesh used for the FEM-indentation in the C45 reference material

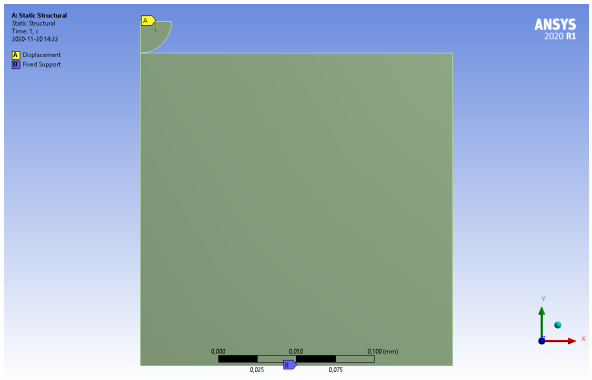

(b) The boundary conditions for the FEM-indentation in the aluminium from Xu and Chen (2010)

Figure 4.6: From ANSYS 2020 R1

The applied boundary conditions were a fixed support at the bottom of the sample and a displacement on the top of the indenter.

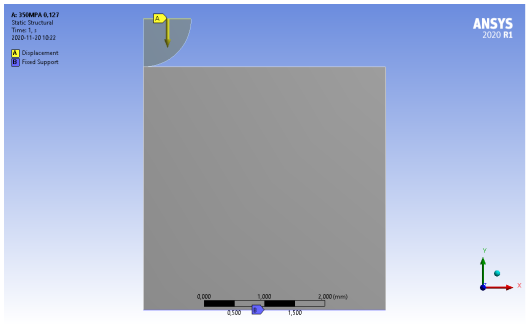

(a) The boundary conditions used for the FEM-indentation in the steel from Xu and Chen (2010)

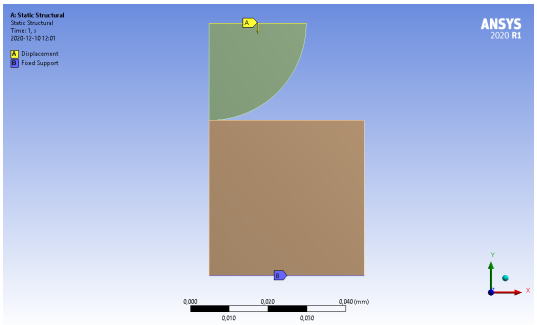

(b) The boundary conditions used for the FEM-indentation in the C45 reference material.

Figure 4.7: From ANSYS 2020 R1

In order to extract the simulated load-depth curves, a table was created in ANSYS showing the reaction force in the applied displacement, as a function of the displacement. This table was then extracted into a text file and imported in Python. The extracted load-depth curves from FEM were then converted to stress-strain curves with the method. The conversion was performed using the values used to create the material model.

4.4 Nanoindentations

4.4.1 General indentation setup

All indentation experiments were performed in a NanoTest Vantage machine from Micro Materials Ltd at the Division of Production and Materials Engineering. The machine was controlled and initial results were extracted using the associated computer with the NanoTest Vantage software.

In the NanoTest Vantage machine, it is possible to perform nanoindentations, microindentations, impact and scratch tests. Different heads are used for the nano- and microindentations, the nanoindentation head can apply loads up to 500 mN, while the microindentation head can apply loads between 0.1 N and 20 N. The experiments can be performed under high temperature, in liquids or in a purged, oxygen free environment. In addition, there is a multi-objective microscope which is used to define the location of a indentation.

All experiments in this thesis have been performed in the nanoindentation head due to availability of a nanoindenter.

Before performing the indentation tests, the sample needs to be cut to an appropriate size, molded into a plastic puck and polished. The puck was then glued to an aluminium cylinder which was then mounted in the machine for the test. The sample was then moved to the microscope where a suitable location for the indentations was chosen before the experiment was started.

After a conducted experiment, the results could be examined in the NanoTest Vantage software. There was also the possibility to perform certain calculations, including the reduced modulus and hardness in the program, although theses parameters have not been the main focus of the thesis. When performing such analysis, the software also compensated for the compliance in the machine and the thermal drift during the indentation. The hysteresis data, showing the corrected load and depth, could then be exported to a text-file. The file was then used in the Python-scripts for converting load-depth data to stress-strain data.

4.4.2 Indentations in C45

Experimental parameters

Before creating the final grid of indentations in the reference material, different experimental parameters were tested in order to build an understanding on how different experimental settings, such as the loading rate, influence the load-depth curves. These tests were necessary since on a nanoscale, all materials exhibit some degree of time dependant effects. These can appear as either viscoelastic effects or as creep.

The tests were performed using parameters within the ranges recommended by the manufacturer of the machine. Only minor differences were found when comparing the loading curves, and the parameters seen in Table 4.2 were chosen for the experiments. The distance between the indentations was chosen to be large enough for the indentations to not be influenced by the plastic zones of earlier indentations.

Experiment setting	**Value**
Max load	500 mN
Loading time	40 s
Unloading time	40 s
Dwell time at max load	20 s
Thermal correction dwell time	60 s
Distance between indentations	30 µm

Table 4.2: Experimental parameters used for the grid in C45

The indentations in the C45 reference material were set up in accordance with Table 4.2. Since the sample rate was constant and the loading rate was constant for all indentations, the average load-depth curve could be calculated by averaging the load and depth for each sample interval.

Results run through the method

In order to analyse the indentations in C45, the initial guess used to calculate the constraint factors were taken from the tensile test and can be seen in 4.3. The iterative procedure was not applied since the calculated stress-strain curve was expected to be in close proximity to the tensile Hollomon curve. The resulting curve can be seen in Figure 5.11.

Material property	**Steel**	**Indenter**
σ_0	331 MPa	-
n	0.216	-
Young's modulus	180 GPa	1141 GPa
Poisson's	0.3	0.07

Table 4.3: Analytical parameters used for the analysis of the C45 reference material.

4.4.3 Indentations in additional materials

In this section, the results from the parts provided by BorgWarner will be shown. The samples were taken from three different components. One hub shaft and one flange made from different types of steel, and an aluminium housing.

The hub shaft had been induction hardened in two regions, where one of the regions included a spline. Therefore, a total of four samples were taken from the cross sections of the hub shaft. One from an unhardened region to be used as a reference for the unhardened material, one in the first hardened region, one in the second hardened region, adjacent to the spline, and one sample from the spline.

The flange had been induction hardened in one region. Therefore only two samples were taken from the flange. One from an unhardened region and one from the hardened region.

The aluminium housing had not been hardened and therefore was only one sample taken from the housing.

Experimental setup

The experimental parameters used can be seen in Table 4.4. They were chosen to be the same as in the C45 reference material, with the exceptions of the minimum distance between indentations and the maximum force when testing aluminium. The distance between indentations was increased to ensure minimal influence from earlier indentations. The maximum load was decreased when performing tests in aluminium since it was expected to not be as hard as the steels.

When testing the hardened samples, experiments were set up as grids, four indentations wide with 250 µm to 300 µm radial increments until the indentations seemed to be within the unhardened region. In the sample with the spline, additional experiments were set up across and along a spline.

Experiment setting	**Value**
Max load	500 mN for steels 300 mN for aluminium
Loading time	40 s
Unloading time	40 s
Dwell time at max load	20 s
Thermal correction dwell time	60 s
Distance between indentations	50 µm

Table 4.4: Experimental parameters used for the samples from BorgWarner.

Analytical setup

Since the method did not deliver accurate results in the C45 reference material, all conversions were performed and presented with the initially assumed values of the material parameters. The parameters used to define α and β are found in Table 4.5 below. The parameters used for the steels were taken from the tensile test of the C45 and the parameters for the aluminium were estimated from the material standard.

Material property	**Steel**	**Aluminium**	**Indenter**
σ_0	331 MPa	140 MPa	-
n	0.216	0.1	-
Young's modulus	180 GPa	73 GPa	1141 GPa
Poisson's	0.3	0.3	0.07

Table 4.5: Analytical parameters used for the analysis of the indentations made in the samples from BorgWarner.

4.5 Data management

After a nanoindentation experiment had been performed, the experimental results were analysed in the corresponding NanoTest Vantage software, and thermal drift and frame compliance was compensated for. After the analysis was performed, the hysteresis data showing the load and depth were exported to text-files. The text-files were then read by a class created in Python and the implementation of the method could begin.

In order to implement the method, a number of scripts were created in Python. The scripts can be seen in Table 4.6 below.

Class	**Brief description**
Main	Used to run all subsequent classes
hysteresis_data_handler	Reads files with load-depth data
fem_data_handler	Reads files with load-depth data from FEM
AlphaBetaCalculator	Calculates the value of α and β from the material parameters
ld_to_eng	Converts load-depth curves to stress-strain curves
StressStrainCalc	Calculates a Hollomon fitting to the stress-strain curve

Table 4.6: Overview of the scripts used when implementing the method

Firstly, the *Main*-class is used to call the other classes and produce plots and other outputs. The reasoning behind is to enable an easier overview of the classes.

Secondly, the classes *hysteresis_data_handler* and *fem_data_handler* are used to read and handle the text-files with the load-depth curves. *Hysteresis_data_handler* also features a couple of extra functionalities, such as calculating the average load-depth curves, correcting eventual depth offset and being able to chose and exclude particular curves.

Furthermore, the *AlphaBetaCalculator*-class calculates the values of α and β based on material parameter input.

The class *ld_to_eng* provides the conversion between load-depth curves to stress-strain curves. Included are several different contact depth calculations, as well as the possibility to calculate the reduced modulus.

Finally, the *StressStrainCalc*-class is used to first convert engineering stress-strain to true stress-strain. The converted stress and strain are then fitted to the Hollomon power-law. An additional feature is the possibility to calculate the 0.2% plastic strain definition of the yield strength.

5. Results

This chapter concerns the experimental results. Firstly, the results of the tensile testing are presented after which the results from the SEM are presented. Subsequently, results from indentations performed in FEM will be presented. Then the results of the reference material will be presented, followed by the material provided by BorgWarner.

5.1 Tensile test

5.1.1 Results

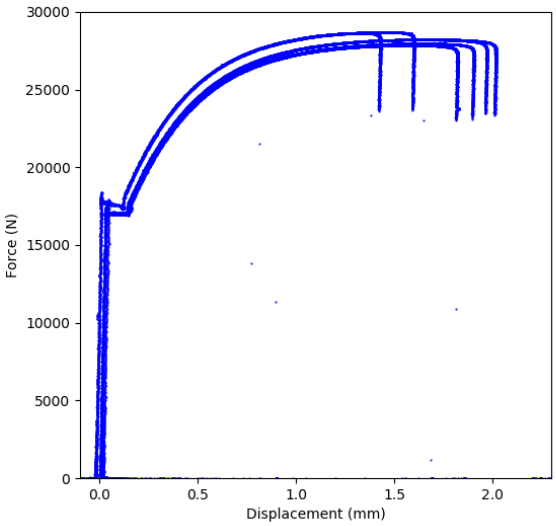

Figure 5.1: The unprocessed data from the tensile test showing the displacement and the applied force.

5.1.2 Curve fitting

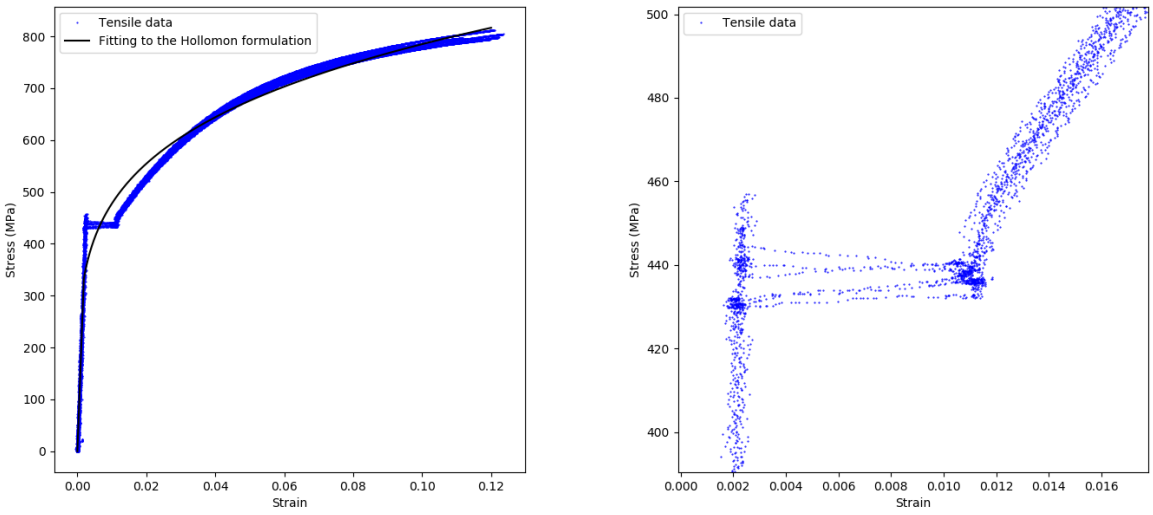

(a) Stress-strain curves from the tensile test (blue) and a least squares fitting of the Hollomon formulation (black).

(b) Image of the Lüder plateau in the C45 reference material

Figure 5.2: From tensile tests

5.2 SEM images

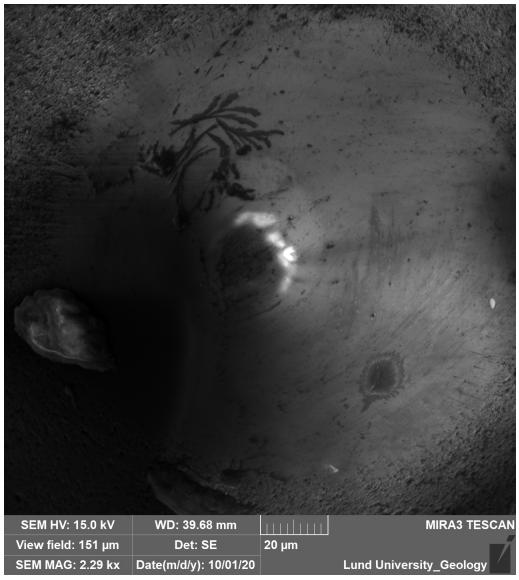

(a) The indenter seen from the above.

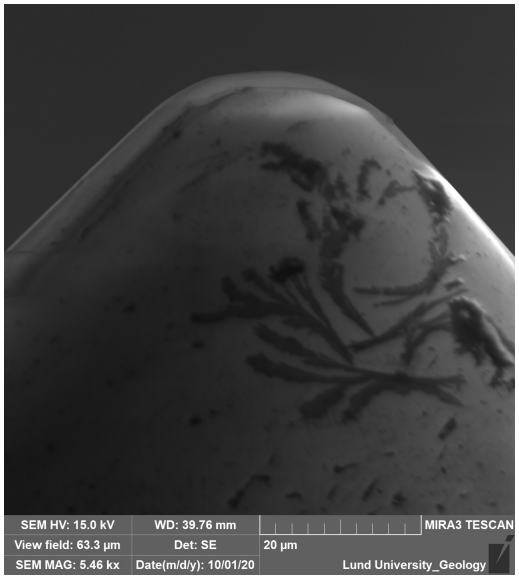

(b) The indenter seen from the side at a 90° angle.

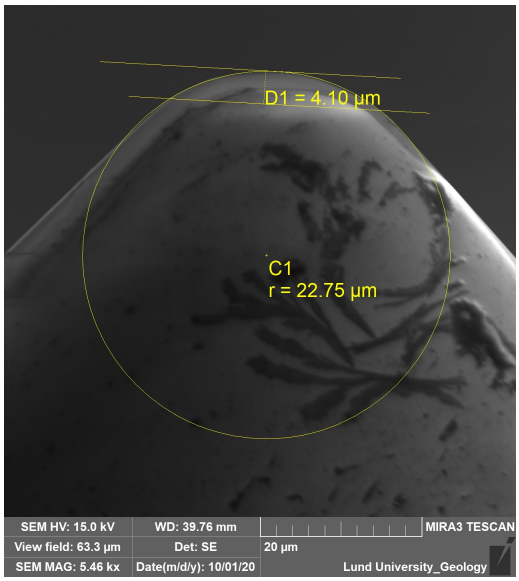

(c) Same image as (b), but with measurements of the radius, 22.75 µm, and two lines showing how far down 4.1 µm is on the indenter. This can be seen in relation to the maximum measured depths of about 1.5 µm.

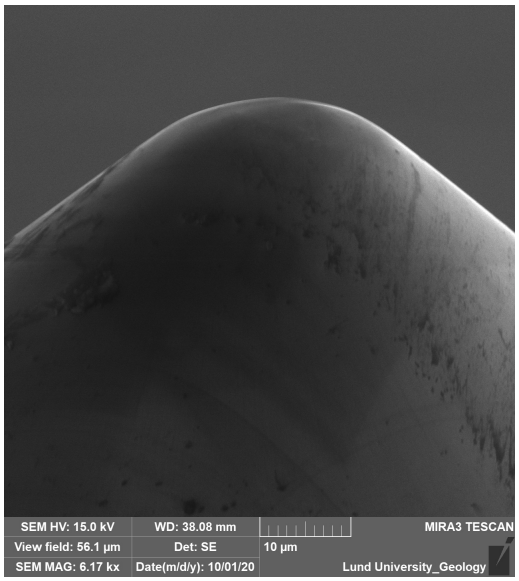

(d) Image of the indenter taken from the side at a 60° angle.

Figure 5.3: Images of the indenter taken with a scanning electron microscope

5.3 FEM results

5.3.1 Stress distribution in C45

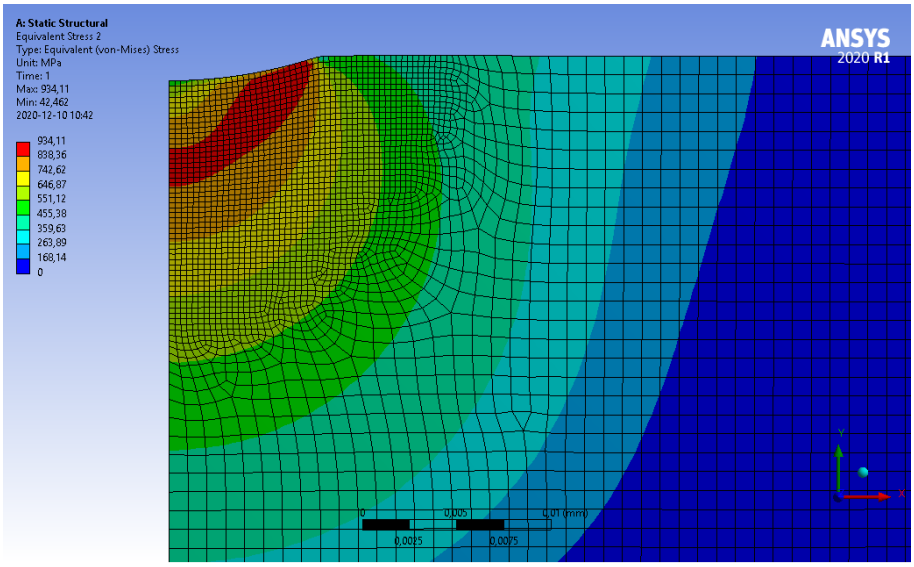

Figure 5.4: The stresses in the C45 when the indenter has reached its maximum depth of 1.35 µm

5.3.2 Load-depth curves

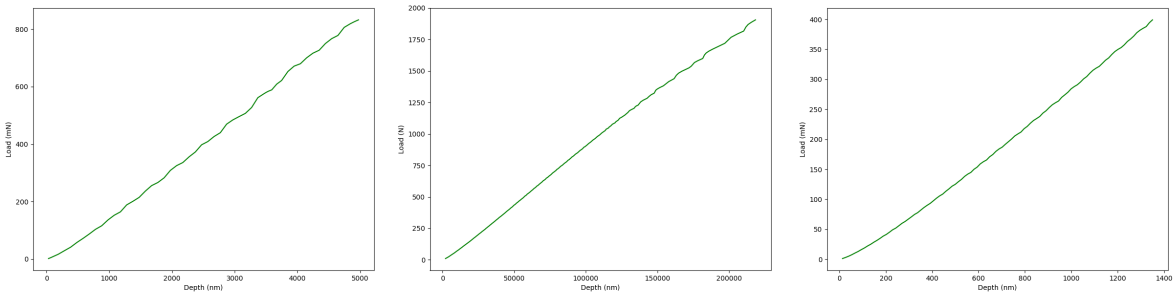

(a) A2024 aluminium, used in the referential article by Xu and Chen (2010)

(b) A533-B steel, used in the referential article by Xu and Chen (2010)

(c) C45, reference material

Figure 5.5: Load-depth curves from indentation made in FEM

5.3.3 Results from FEM run through the method

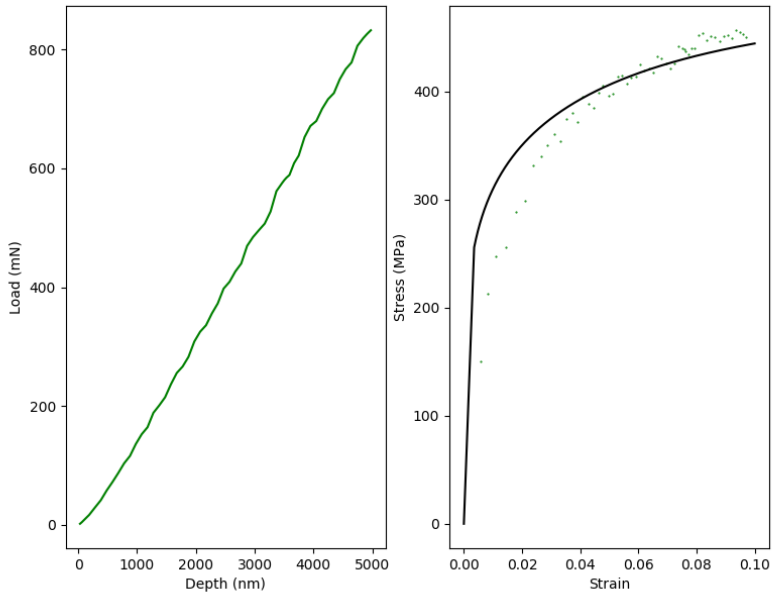

Figure 5.6: The load-depth curve from the FEM-indentation in the A2024 aluminium from Xu and Chen (2010) and its conversion to stress and strain (green points) compared to the stress-strain curve used in the simulation (black line).

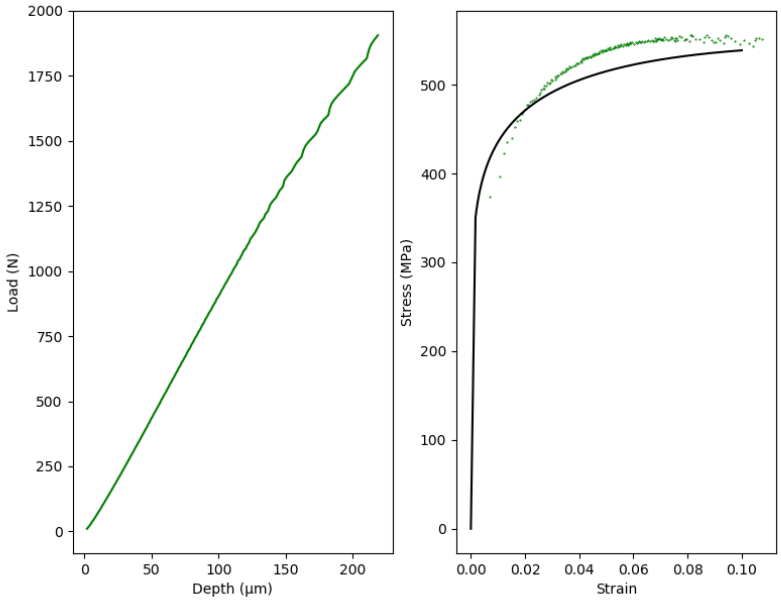

Figure 5.7: The load-depth curve from the FEM-indentation in the A533-B steel from Xu and Chen (2010) along with its stress-strain conversion (green points) compared to the stress-strain curve used in the simulation (black line).

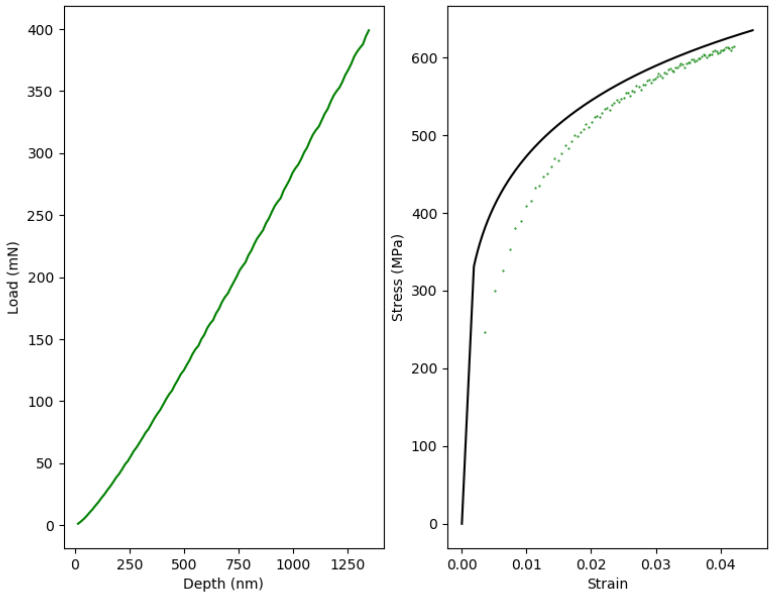

Figure 5.8: The load-depth curve from the FEM-indentation in the C45 reference material and its conversion into stress and strain (green points) compared to the stress-strain curve from the tensile test (black line).

5.4 Experimental results, reference material

5.4.1 Indentation results from the grid in C45

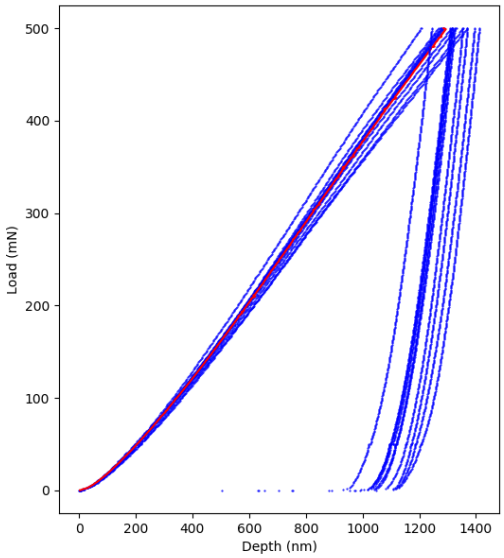

Figure 5.9: Load-depth curves from the C45 steel (blue) and the average load-depth curve (red).

5.4.2 Experimental results compared with FEM results

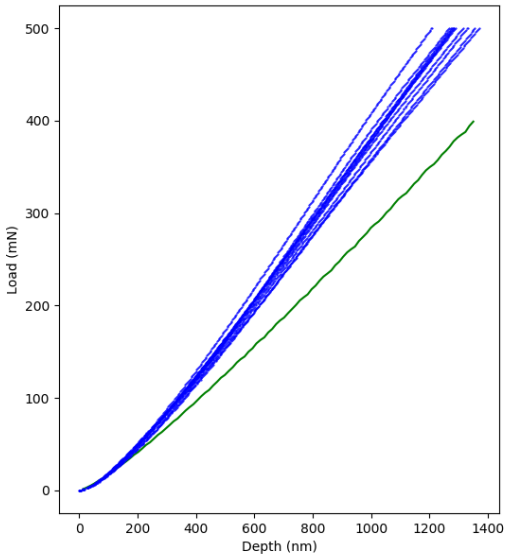

Figure 5.10: Loading curves from the experimental indentations in C45 steel (blue) and the simulated indentation curve (green).

5.4.3 Results run through the implemented method

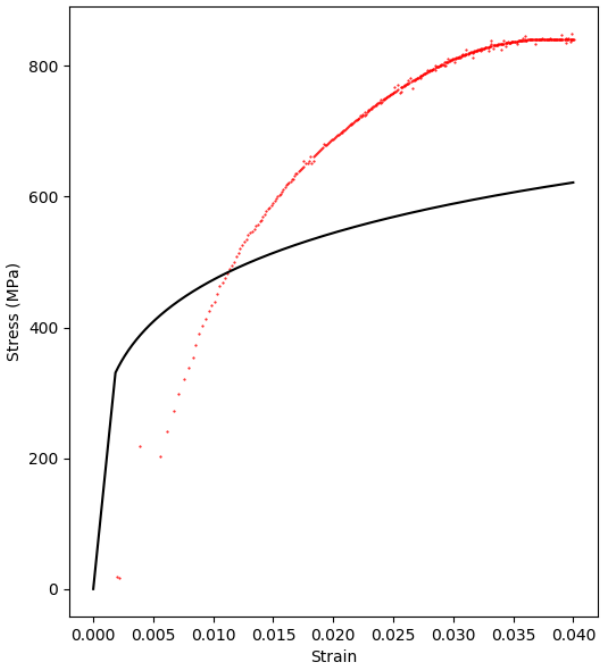

Figure 5.11: Stress-strain curve from the average load-depth curve (red) compared to the Hollomon curve from the tensile test (black).

5.4.4 Microscope image

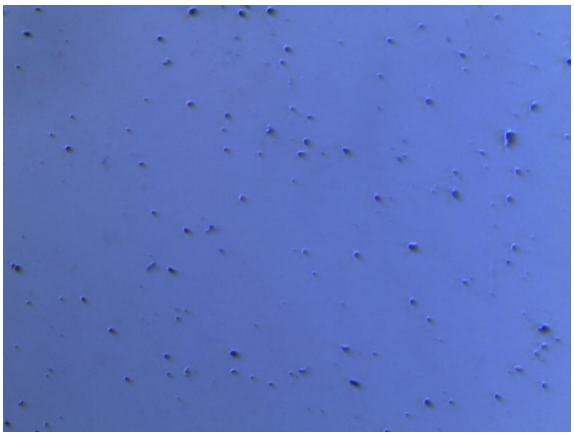

Figure 5.12: Image of the microstructure of the C45 reference material.

5.5 Experimental results, other materials

5.5.1 Hub shaft, unhardened region

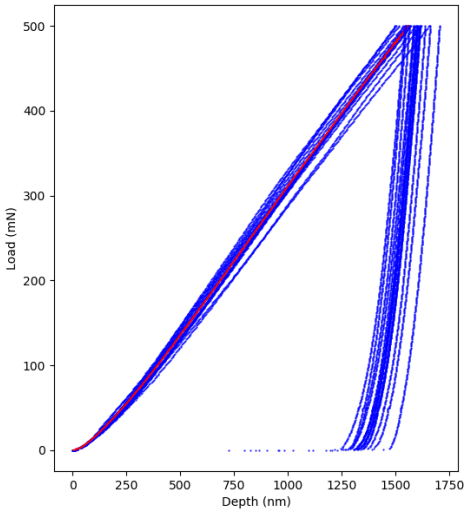

(a) Load-depth curves in an unhardened section of the hub shaft (blue) and an average curve (red)

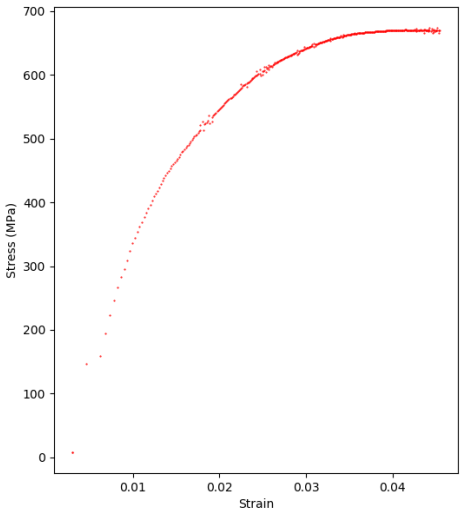

(b) stress-strain curve from the unhardened section of hub shaft.

Figure 5.13: Results from the indentations in the unhardened region of the hub shaft

5.5.2 Hub shaft, first hardened region

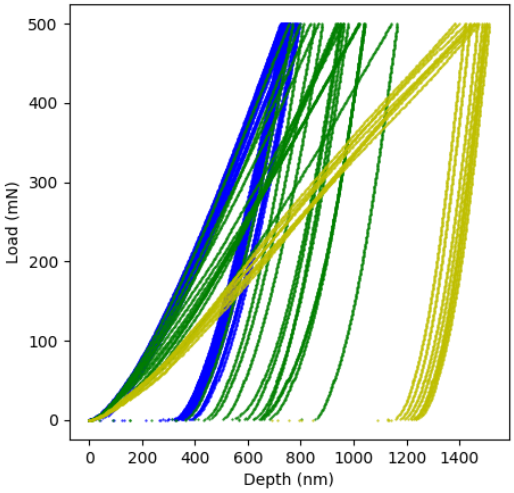

(a) Load-depth curves from the first hardened section from the hub shaft. The colors correlate to the regions in the section view below.

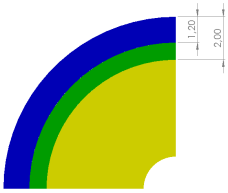

(b) Section view of the first hardened section indicating the radial location of the different indentations.

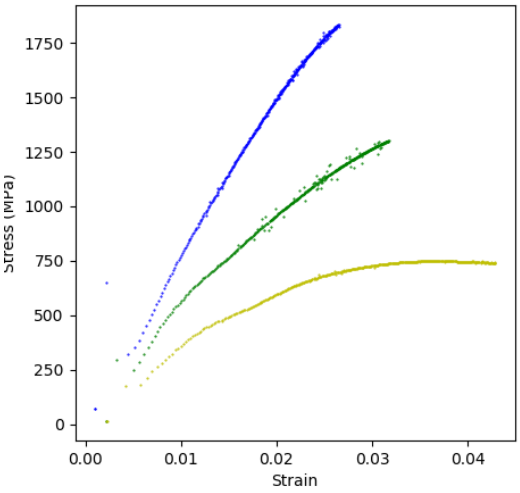

(c) Stress-strain curves corresponding to the average load-depth curve from the zones above.

Figure 5.14: Results from the indentations in the first hardened section of the hub shaft.

5.5.3 Hub shaft, second hardened region

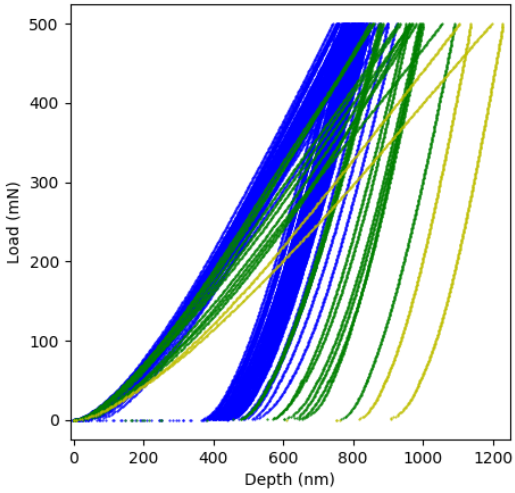

(a) Load-depth curves from the second hardened section from the hub shaft. The colors correlate to the regions in the section view below.

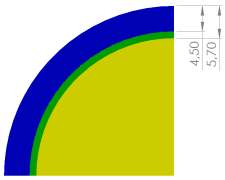

(b) Section view of the second hardened section indicating the radial location of the different indentations.

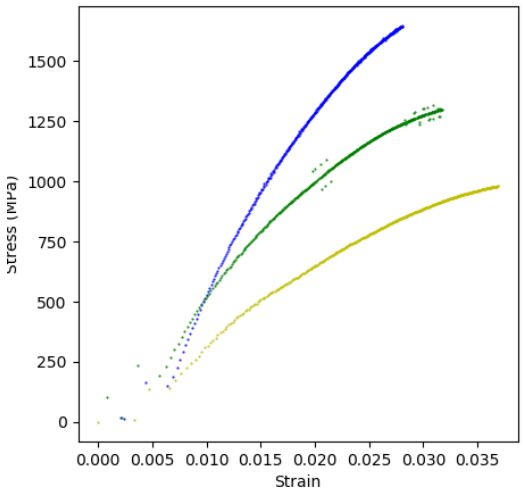

(c) Stress-strain curves corresponding to the average load-depth-curve from the zones above.

Figure 5.15: Results from the indentations in the second hardened section of the hub shaft.

5.5.4 Hub shaft, hardened region with spline

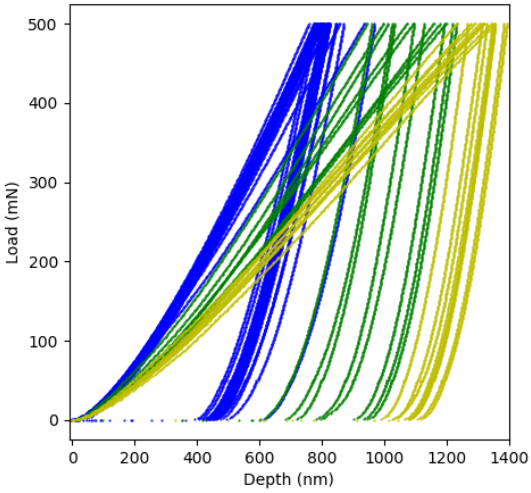

(a) Load-depth curves from the hardened section with the spline from the hub shaft. The colors correlate to the regions in the section view below.

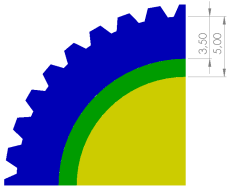

(b) Section view of the hardened section with the spline indicating the radial location of the different indentations.

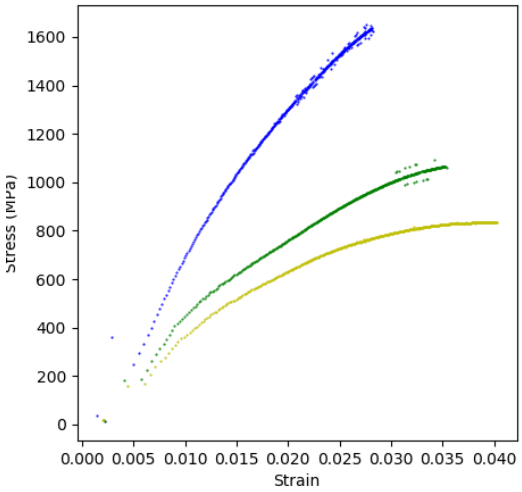

(c) Stress-strain curves corresponding to the average load-depth-curve from the zones above.

Figure 5.16: Results from the indentations in the hardened section with the spline on the hub shaft.

5.5.5 Flange, unhardened region

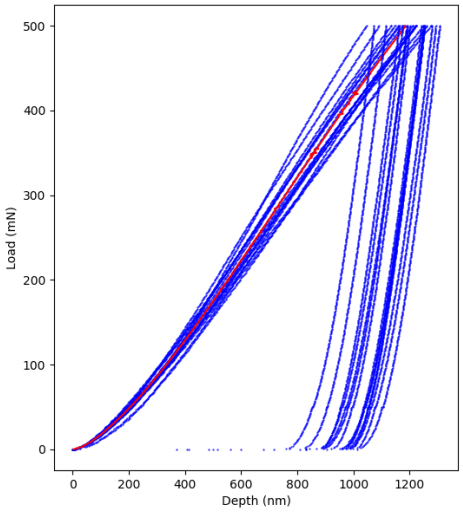

(a) Load-depth curves in a unhardened section of the flange.

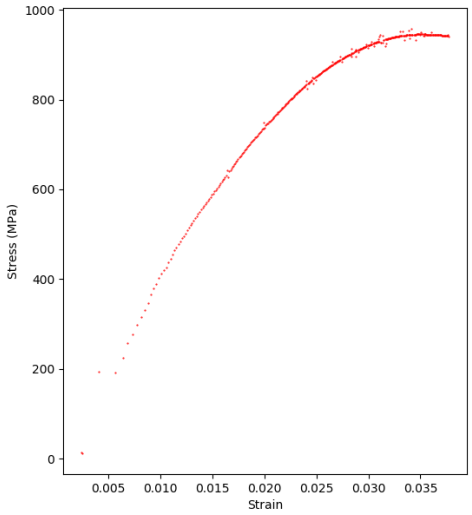

(b) Average stress-strain curve from the unhardened section of the flange.

Figure 5.17: Results from the indentations in the unhardened region of the flange.

5.5.6 Flange, hardened region

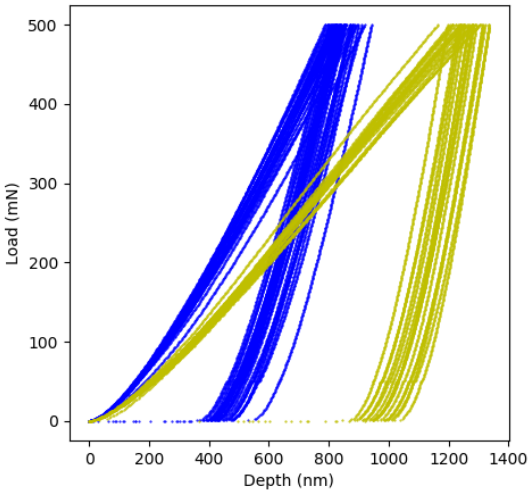

(a) Load-depth curves from the hardened section from the flange. The colors correlate to the regions in the section view below.

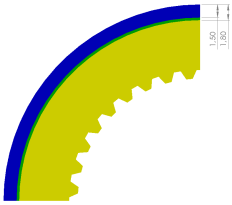

(b) Section view of the hardened section of the flange.

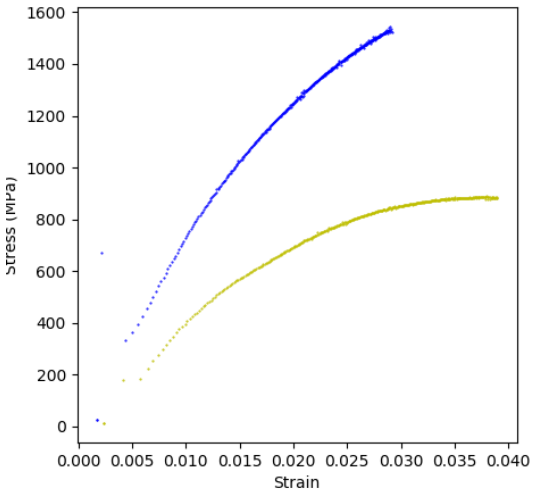

(c) Stress-strain curves corresponding to the average load-depth curve from the zones above.

Figure 5.18: Results from the indentations in the hardened section of the flange.

5.5.7 Aluminium housing

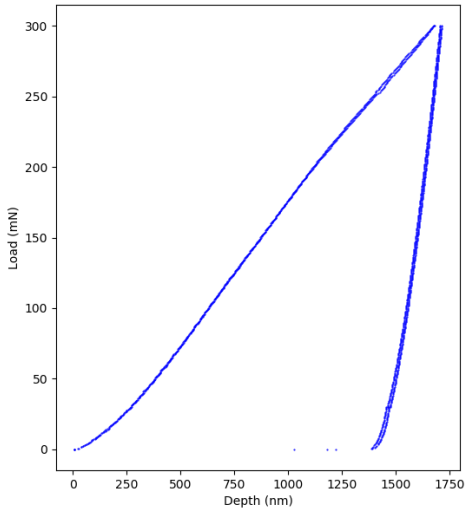

(a) Load-depth curves from the indentations in the aluminium housing.

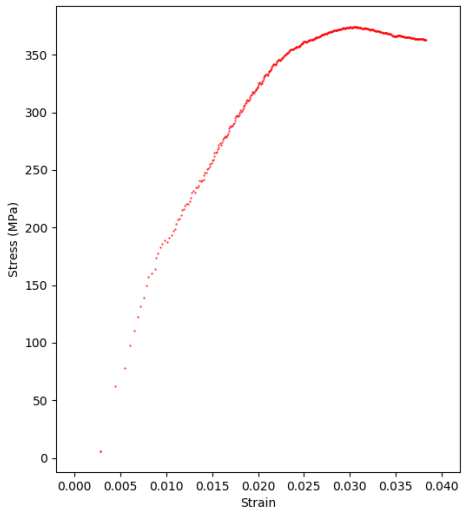

(b) The average converted stress-strain curve for the aluminium housing.

Figure 5.19: Results from the indentations in the aluminium housing.

5.5.8 Microscope images

This section contains microscopic images of the different regions of the samples from the parts from BorgWarner.

Hub shaft

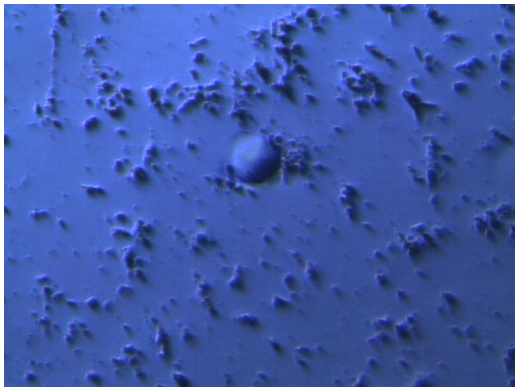

(a) Image of the microstructure and an indentation in the hub shaft in an unhardened region.Taken with 50x magnification.

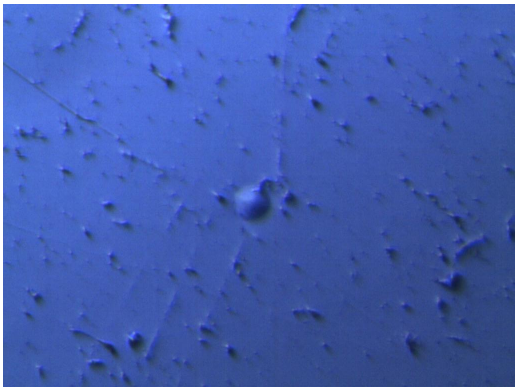

(b) Image of the microstructure and an indentation in the hub shaft in the hardened region of the first section.Taken with 50x magnification.

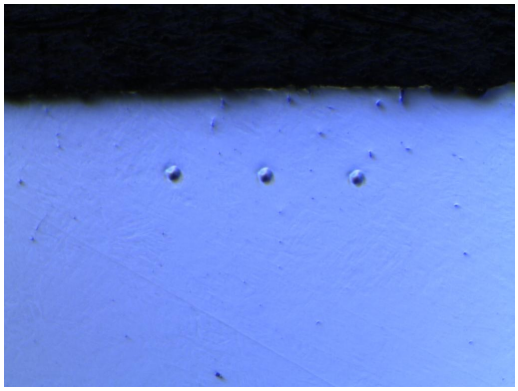

(c) Image of the microstructure and three indentations in the hub shaft in the hardened region of the second section. Taken with 20x magnification.

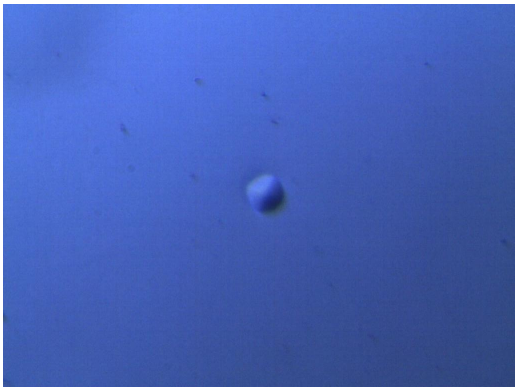

(d) Image of the microstructure and an indentation in the hub shaft in the hardened region of the spline. Taken with 50x magnification.

Figure 5.20: Microstructure of hub shaft

Flange

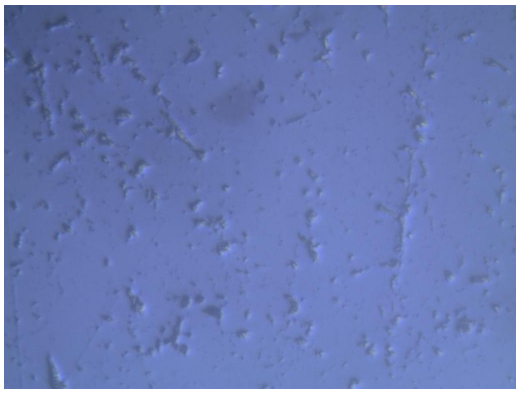

(a) Unhardened region.Taken with 50x magnification.

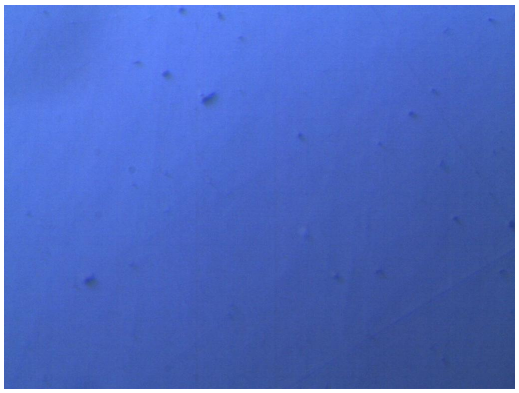

(b) Hardened region of the first section. Taken with 50x magnification.

Figure 5.21: Microstructure of the flange

Aluminium housing

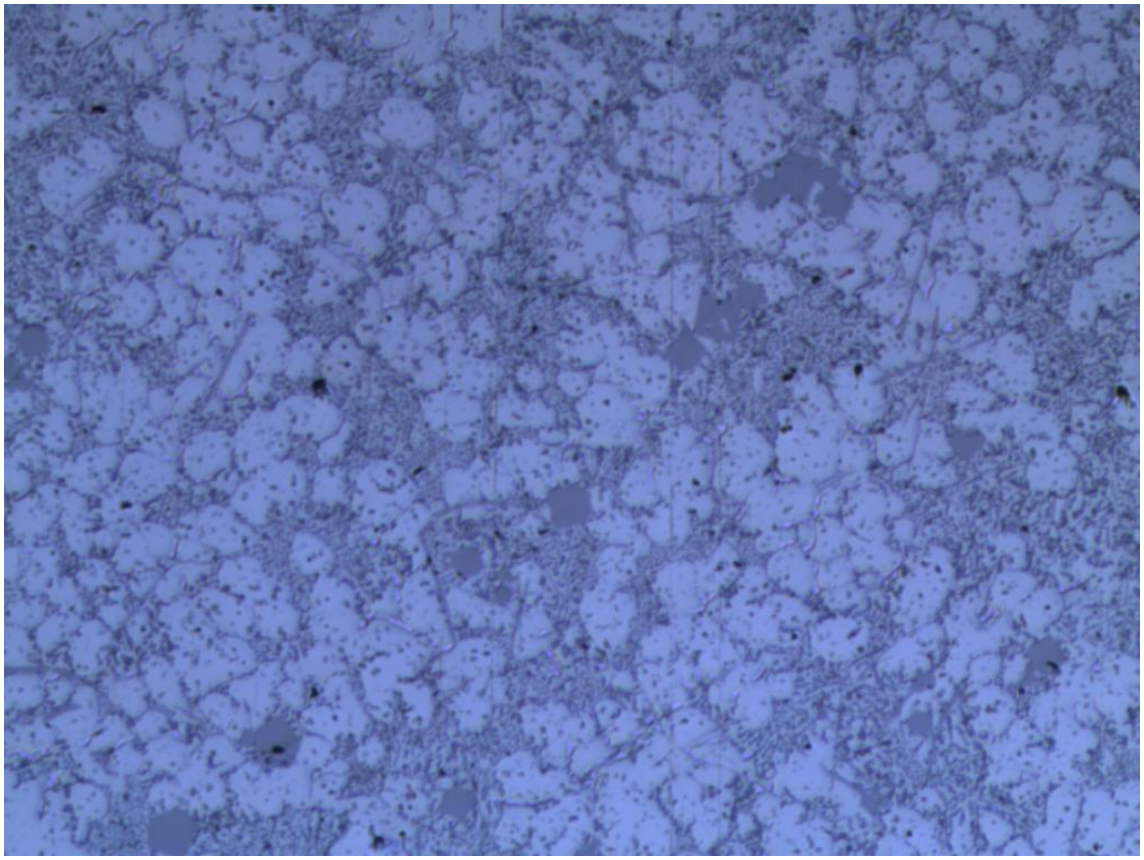

Figure 5.22: Image of the microstructure of the aluminium housing. Taken with 20x magnification.

6. Discussion

This chapter discusses the experimental results of the tensile testing, experimental results from indentation of the reference material and the provided material from BorgWarner as well as the results from simulated indentations done with FEM. It includes experimental as well as conceptual conclusions and a larger chapter on recommendations for further work.

6.1 Conclusions from direct results

6.1.1 Hollomon fitting of tensile test

When the tensile tests were performed, the material showed a very distinct Lüder plateau at 430 MPa, which has been the source of much concern. A Lüder plateau is when a material under tensile testing abruptly stops being linear elastic and instead has a constant stress while continuing to elongate. An enlarged image of the Lüder plateau can be seen in Figure 5.2b.

Since most researcher use the Hollomon equation, including Xu and Chen (2010), Hollomon's formulation was chosen. There are several methods for fitting the plastic parameters in the Hollomon equation. For an ideal material, the strain hardening is defined as the slope of the plastic region of the logarithmical stress-strain curve. This formulation would however lead to difficulties in defining the proportional limit. This Hollomon stress-strain curve would either be a perfect fit in the plastic region and a very low proportional limit, or lead to a constant overestimation of the stress past the proportional limit.

Therefore two types of least squares fittings were evaluated. In the first one, the proportional limit was set to 430 MPa. However, this method led to a relatively bad fit with an overestimation of the stress in the elastic-plastic region and an underestimation of the stress for large strains. The final model was then decided to optimise both the proportional limit and the strain hardening exponent with the least squares procedure.

6.1.2 FEM results

After running the load-depth curves from FEM through the forward analysis procedure, it can be concluded that the method appears to be working as intended. This is however an ideal case where the material behaves as it does in a macroscale since no microstructural considerations were made.

6.1.3 SEM

As stated earlier, the indenter was mounted in a rather arbitrary way and it was not possible to achieve a 90° view of the indenter on all sides without needing to remount the indenter for every image. Therefore, only one setup at 90° was performed, and the subsequent images were taken at a 60° angle from all sides.

Some measurements were made of the tip radius, but due to the arbitrary mounting method, they are not accurate enough to determine a definite radius. Although it is likely that the measurement is close to the real value. It could also be concluded that the indenter does not suffer from any significant damage to the tip where the indentations have been performed.

6.1.4 General indentation results

When performing indentations in any material, the indenter occasionally hit pores, graphite grains or dust particles. All of these lead to irregular load-depth curves which generate higher or lower hardness and modulus values, as well as stress-strain results after being processed by the method. These irregular indentations have generally been removed before final processing.

It is generally suggested that at least five indentations should be performed in a material or a region in order to get a good average of the zone. This is then weighed against the wear every indentation causes on the indenter. Therefore, it was decided to perform fifteen indentations in the C45 reference material, as well as the samples which had not been heat treated.

6.1.5 Indentations in C45

The indentations in the C45 reference material were rather consistent with a reasonable distribution around the mean curve. There were however a couple of curves which appeared to be in pores causing them to deviate significantly.

As seen in Figure 5.11 that the method fails to accurately describe the tensile properties of the reference material It can also be noted that the experimental curves and the simulated curve differ significantly. This can be seen in Figure 5.10.

6.1.6 Experimental results from BorgWarner materials

Hardened steel

Although the method failed to estimate the stress-strain curve of the reference material, indentations were conducted in the material samples from BorgWarner. The study of these materials became a relative study showing how the different sections behave in relation to each other. The setup was created in the same manner as in the reference material, with the exception of an increased distance between indentations due to the unknown nature of the materials and in order to reduce the number of needed indentations.

In the analyses of the hardened samples, it can be seen that in the hardened region, the stress-strain curves does not seem to transition into the fully plastic region. It is therefore not even possible to perform a curve fitting on the curve, and therefore not possible to initiate the iterative reverse analysis. Therefore, all

analyses of the indentations in steel were performed with the α and β from the tensile test of the reference material.

With these generated values, it is possible to create approximate heat maps showing region with roughly the same material properties. From these heat maps, it is possible to draw the conclusion that the induction hardening creates a zone with rather homogeneous properties down to a certain depth from the surface of the part, after which a short transition region follows before the material is fully unhardened. This transition is particularly short in the flange where no indentations appeared inside the transition region, the indentation were made with 300 µm in radial increments.

Aluminium

The aluminium is a multi phase material which would require more analysis in order to evaluate the influence of the different phases. A systematic design of grids would have to be structured in order to extract an average of mechanical properties due to the different phases behaving differently in an indentation procedure. Since microstructural influences was not a main focus point for this thesis the indentation data provided to BorgWarner from the aluminium will have to be further analysed with respect to the different phases and its overall different microstructure.

This particular aluminium alloy is a relatively brittle alloy that might be stronger in compression than in tension. It is unclear how the different properties would influence the indentations and the conversion to stress and strain.

6.2 Conceptual conclusions

6.2.1 Microstructural influences

Pile-up & sink-in

Concerning the calculation of contact depth in an indentation the microstructural phenomena pileup and sink-in play an important role, since it will define the contact depth radius of the indenter and thus the conversion of indentation load and depth to stress-strain data. It concerns the relation between the elastic recovery depth and the maximum penetration depth, the latter measured experimentally and the elastic recovery meant to be compensated for analytically. The phenomena depends on the mechanical properties of the material, more specifically the Young´s modulus to yield strength ratio, the strain hardening exponent and friction (Xu 2004).

The ratio of Young's modulus and yield strength for the C45 steel is, approximately 544, which is sufficiently high to expect the material to show some pile-up during indentation. Sink-in is mainly shown in materials with a low Young's modulus to yield strength ratio and low strain hardening exponent. The contact area can therefore be underestimated with materials that show the pile-up phenomenon to up to 60 percent and cause the hardness to be gravely overestimated.

Indentation size effect

The deformation mechanisms of plasticity in crystalline material can, as mentioned, cause an effect called indentation size effect. This is because of geometrically nec-

essary dislocations that occur in the plastic zone of indentation. At shallow depths, too few of the geometrically necessary dislocations occur to enable the material flow when experiencing deformation. The phenomenon seems to be less prominent with spherical indenters that have a radius that is larger than 100 µm (Pharr, Herbert, and Gao 2010). The radius of the chosen indenter should then be chosen taking indentation size effect into consideration.

6.2.2 Experimental results

Based on the results in the reference material and the works by Pharr, Herbert, and Gao (2010), it seem likely that the geometrical circumstances cause a stiffer response due to the indentation size effect. Since it is a purely geometrical effect it would need a new indenter in order to be counteracted. It might be possible to analytically compensate for the effect but would require more research and might be material dependant.

Errors might also occur due to different properties in tensile and compression. Even if the bulk material has homogeneous properties, there might be anisotropic grains or particles within the material which are missed by the nanoindentations. The pores and particles causing irregular behaviours on certain load-depth curves might be part of the reason why the experiments seem to require a higher load than the FEM simulations.

The Lüder planes in the material, which caused the plateau in the tensile test, might influence the behaviour of the plastic zone. If the planes influence the plastic zone around the indenter, they are likely to be a part of the reason behind the stiffer response.

It can be noted that several of the stress-strain curves from the experimental indentations seem failing to reach the origin. The reason for that phenomena can be a number of things, but might come from the calibration of the origin. The depth offset at zero load should be corrected, but since the correction is based on the initial curve, any influence on the initial curve will influence the offset correction. Influencing factors can be sliding during the initial contact before penetration, rough surface roughness and work hardening in the surface can affect the results, although the effects of these factors are unclear.

Furthermore, it is assumed that the friction only plays a minor role in the indentation process until larger depths. There seems to be a rather wide consensus regarding the friction. Few researchers in general assume a higher friction coefficient than approximately 0.1.

6.3 Further work

6.3.1 Microstructure

Pile-up and sink-in As discussed concerning conclusions of microstructural influences, the pile-up and sink-in phenomena can contribute in great part to the overestimated stresses. A further recommendation is to investigate the specific experimental parameters of materials similar to those of unknown mechanical properties to be able to accurately take these phenomena into account. The contact

area can, as an example, be calculated from direct imaging using atomic force microscopy(AFM) then looking at the residual impression.

6.3.2 Microindentation

As stated earlier, the indentation size effect seems to be causing errors in the experiments performed in this thesis. It would therefore be necessary to research how the indentation size effect influences the indentations before proceeding with any research.

Even if it is found that the errors can be compensated, it would be recommended to change indentation type. This is due to the indentations in the hardened steels not being able to penetrate deeper due to insufficient force in the nanoindentation head.

Our recommendation would therefore be to proceed with our research with a larger indenter in the microindentation head in the NanoTest Vantage machine.

6.3.3 Use of Machine Learning algorithm

An interesting alternative to the analytical method is to explore the possibility of using a Multi-Fidelity Neural Network as described in the chapter Theory of this report. As seen in the results of the study by Lu et al. (2020) the accuracy is drastically improved when combining different types of sets of data, both low and high fidelity data and in combination with a boosting of the high fidelity subnetwork with experimental data sets from material close to the material of unknown properties.

There would also be an advantage in making use of transfer learning for training of the neural network, because of its possibility to continue boosting the high fidelity subnetwork with new experimental data when necessary.

The transfer learning shows improved accuracy in results of determining yield strength. Lu et al. (2020) present an analysis of two aluminium alloys (Al7075-T651, Al6061-T6511) and two 3D-printed titanium alloys (B3067, B3090).

It would be a current way of researching the new possibilities presented with using a vast amount of data to create a robust system, without having to invest in the relatively expensive extensive experimental indentation data when small amounts of experimental data from materials similar to that of the material with unknown properties are necessary. Thereby, the system can be continuously used for different kinds of material with the same level of accuracy in the future.
In order to create a robust neural network based on both low and high fidelity simulation data, meaning both 2D and 3D FEM simulations of indentation, effort will need to be put on examining the optimal FEM parameters for effective simulation to keep making use of a lower need for processing power.

Bibliography

Ahn, Jeong-Hoon and Kwon, Dongil (2001). "Derivation of plastic stress–strain relationship from ball indentations: Examination of strain definition and pileup effect". In: *Journal of Materials Research* 16.11. DOI: 10.1557/JMR.2001.0437, pp. 3170–3178.

Beghini, M., Bertini, Leonardo, and Fontanari, Vigilio (Apr. 2006). "Evaluation of the stress–strain curve of metallic materials by spherical indentation". In: *International Journal of Solids and Structures - INT J SOLIDS STRUCT* 43. DOI: 10.1016/j.ijsolstr.2005.06.068, pp. 2441–2459.

Blaoui, Mossaab, Zemri, Mokhtar, and Abdessamad, Brahami (Jan. 2018). "Effect of Heat Treatment Parameters on Mechanical Properties of Medium Carbon Steel". In: *Mechanics and Mechanical Engineering* 22, pp. 909–918.

Bouzakis, K.-D, Michailidis, Nikolaos, and Erkens, G. (July 2001). "Thin hard coatings stress–strain curve determination through a FEM supported evaluation of nanoindentation test results". In: *Surface and Coatings Technology* 142, pp. 102–109. DOI: 10.1016/S0257-8972(01)01275-0.

Chang, Chao et al. (Feb. 2018). "Representative Stress-Strain Curve by Spherical Indentation on Elastic-Plastic Materials". In: *Advances in Materials Science and Engineering* 2018. DOI: 10.1155/2018/8316384, pp. 1–9.

Chung, Kyung-Hwan et al. (Jan. 2009). "Characterization of mechanical properties by indentation tests and FE analysis-validation by application to a weld zone of DP590 steel". In: *International Journal of Solids and Structures - INT J SOLIDS STRUCT* 46, pp. 344–363. DOI: 10.1016/j.ijsolstr.2008.08.041.

De Bono, Damaso (July 2017). "Inverse analysis and microstructure effects in nanoindentation testing." Available online: http://epubs.surrey.ac.uk/841572/. PhD thesis. University of Surrey.

De Bono, Damaso et al. (Feb. 2017). "A robust inverse analysis method to estimate the local tensile properties of heterogeneous materials from nano-indentation data". In: *International Journal of Mechanical Sciences* 123, pp. 162–176. DOI: 10.1016/j.ijmecsci.2017.02.006.

Haj-Ali, Rami et al. (Mar. 2008). "Nonlinear constitutive models from nanoindentation tests using artificial neural networks". In: *International Journal of Plasticity* 24, pp. 371–396. DOI: 10.1016/j.ijplas.2007.02.001.

Hertz, Heinrich (1882). "On the Contact of Elastic Solids". In: *Crelle's Journal* 92, pp. 156–171.

Hollomon, John H. (1945). "Tensile Deformation". In: *American Institute of Mining and Metallurgical Engineers* 1879.

Iracheta, Omar, Bennett, Chris, and Sun, Wei (Jan. 2016). "Characterisation of material property variation across an inertia friction welded CrMoV steel com-

ponent using the inverse analysis of nanoindentation data". In: *International Journal of Mechanical Sciences* 107. DOI: 10.1016/j.ijmecsci.2016.01.023.

Jeong, HyeokJae et al. (Dec. 2014). "Local and Global Stress–Strain Behaviors of Transformation-Induced Plasticity Steel Using the Combined Nanoindentation and Finite Element Analysis Method". In: *Metallurgical and Materials Transactions A* 45, pp. 6008–6015. DOI: 10.1007/s11661-014-2544-2.

Khan, Muhammad Kashif et al. (Oct. 2010). "A combined experimental and finite element approach for determining mechanical properties of aluminium alloys by nanoindentation". In: *Computational Materials Science* 49, pp. 751–760. DOI: 10.1016/j.commatsci.2010.06.018.

Lu, Lu et al. (2020). "Extraction of mechanical properties of materials through deep learning from instrumented indentation". In: *Proceedings of the National Academy of Sciences* 117.13, pp. 7052–7062. ISSN: 0027-8424. DOI: 10.1073/pnas.1922210117. eprint: https://www.pnas.org/content/117/13/7052.full.pdf. URL: https://www.pnas.org/content/117/13/7052.

Meng, Xuhui and Karniadakis, George (Oct. 2019). "A composite neural network that learns from multi-fidelity data: Application to function approximation and inverse PDE problems". In: *Journal of Computational Physics* 401, p. 109020. DOI: 10.1016/j.jcp.2019.109020.

Min, Li et al. (Jan. 2004). "A numerical study of indentation using indenters of different geometry". In: *Journal of Materials Research* 19, pp. 73–78. DOI: 10.1557/jmr.2004.19.1.73.

Nix, William D. and Gao, Huajian (1998). "Indentation size effects in crystalline materials: A law for strain gradient plasticity". In: *Journal of the Mechanics and Physics of Solids* 46.3, pp. 411–425. ISSN: 0022-5096. DOI: https://doi.org/10.1016/S0022-5096(97)00086-0. URL: http://www.sciencedirect.com/science/article/pii/S0022509697000860.

Oliver, W.C. and Pharr, G.M. (1992). "An improved technique for determining hardness and elastic modulus using load and displacement sensing indentation experiments". In: *Journal of Materials Research* 7.6. DOI: 10.1557/JMR.1992.1564, pp. 1564–1583.

Pharr, George, Herbert, Erik, and Gao, Yanfei (July 2010). "The Indentation Size Effect: A Critical Examination of Experimental Observations and Mechanistic Interpretations". In: *Annual Review of Materials Research* 40, pp. 271–292. DOI: 10.1146/annurev-matsci-070909-104456.

Schuh, Christopher A. (2006). "Nanoindentation studies of materials". In: *Materials Today* 9.5, pp. 32–40. ISSN: 1369-7021. DOI: https://doi.org/10.1016/S1369-7021(06)71495-X. URL: http://www.sciencedirect.com/science/article/pii/S136970210671495X.

Shield, R. T. (1955). "On the plastic flow of metals under conditions of axial symmetry". In: *Proceedings of the Royal Society of London. Series A. Mathematical and Physical Sciences* 233, pp. 267–287.

Sneddon, Ian N. (1965). "The relation between load and penetration in the axisymmetric boussinesq problem for a punch of arbitrary profile". In: *International Journal of Engineering Science* 3.1, pp. 47–57. ISSN: 0020-7225. DOI: https://doi.org/10.1016/0020-7225(65)90019-4. URL: http://www.sciencedirect.com/science/article/pii/0020722565900194.

Tabor, D. (1951). "The Hardness of Metals". In: *Monographs on the Physics and Chemestry of Materials*. Ed. by N. F. Mott Willis Jackson H. Fröhlich. viewed November 10 2020,URL: https://archive.org/details/TaborHardnessOfMetals/page/n1/mode/2up. Oxford: Clarendon Press.

Taljat, B., Zacharia, T., and Kosel, F. (1998). "New analytical procedure to determine stress-strain curve from spherical indentation data". In: *International Journal of Solids and Structures* 35.33, pp. 4411–4426. ISSN: 0020-7683. DOI: https://doi.org/10.1016/S0020-7683(97)00249-7. URL: http://www.sciencedirect.com/science/article/pii/S0020768397002497.

Valiev, R. Z. et al. (2007). "The Innovation Potential of Bulk Nanostructured Materials". In: *Advanced Engineering Materials* 9.7, pp. 527–533. DOI: 10.1002/adem.200700078. eprint: https://onlinelibrary.wiley.com/doi/pdf/10.1002/adem.200700078. URL: https://onlinelibrary.wiley.com/doi/abs/10.1002/adem.200700078.

Xu, Baoxing and Chen, Xi (2010). "Determining engineering stress–strain curve directly from the load–depth curve of spherical indentation test". In: *Journal of Materials Research* 25.12, pp. 2297–2307. DOI: 10.1557/jmr.2010.0310.

Xu, Zhi-Hui (2004). "Mechanical Characterisation of Coatings and Composites-Depth-Sensing Indentation and Finite Element Modelling". PhD thesis. Stockholm, Sweden: Department of Materials Science and Engineering Royal Institute of Technology.

7. Appendix: Popular scientific abstract

Material science:
Using Nanoindentation to draw big conclusions

When streamlining material models in the production industry there is a need to achieve energy efficiency and reduce carbon dioxide emissions, achievable partly by optimising component production. Implementing current research of Nanoindentation at BorgWarner makes it possible to try new techniques of determining material properties directly on components used in the industry today.

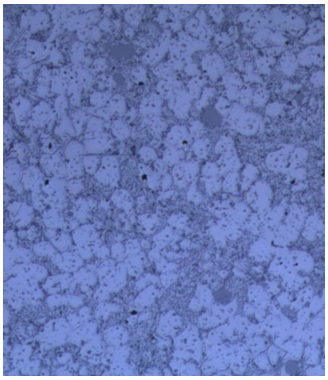
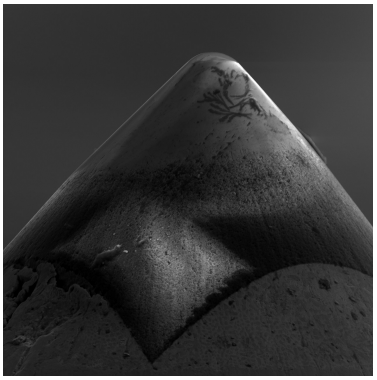
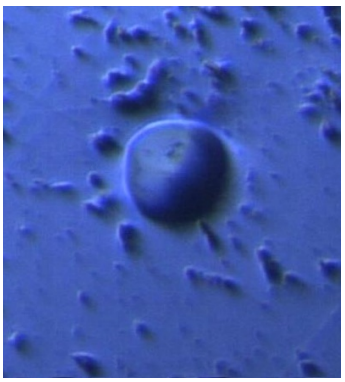

From left to right: The microstructure of an aluminium alloy, a nanoindenter with a tip radius of 25 µm, and the residual imprint after a nanoindentation.

The standard procedure for determining the strength of a material, is by performing a tensile test. A tensile test is when a sample of a material is pulled until breaking, and results in a stress-strain curve showing the strength of the material. However, a tensile test can only provide the average material behaviour, which is enough for most materials. But not all materials are properly represented by the average strength. For instance, if a material has been partially heat treated to make it stronger in certain segments, as is the case with this project, a tensile test would still only provide the average properties of the material. To be able to provide accurate data of the different regions, the thesis[1] aims to estimate the varying strengths by using nanoindentations.

A nanoindentation is performed with a small indenter, usually in the shape of a cone, sphere or a pyramid. This indenter is used to perform a small dent in the material. The indentation is typically performed up to a depth of approximately 1 µm. The output from a nanoindentation is a load-depth curve showing the force needed to reach certain depths and provide useful information about the elasticity of the material. It is then possible to estimate the strength of the material using various methods for relating the load-depth curve to the stress-strain curve.

The method used in the thesis[1] to translate the data from indentation to a larger material perspective, is an analytical method based on the works by Xu and Chen.[2] It is a mathematical method derived from classical contact mechanics and geometrical relationships. Analytical methods are, because of them being based in these basic relationships, desirable to use, but also problematic because of their inherent inability to compensate for deviations in experimental settings.

The experimental environments sensitive nature, acting on a nanoscale and thereby trying to circumvent the significant microstructural influences, led to inconclusive results. But the method showed great promise in being able to compare the strengths of distinct regions of material as well as different materials to one another, which can be used by the company today.

For the future, the thesis[1] recommends BorgWarner to also look into an exciting possibility to incorporate Machine Learning Algorithms into the handling of experimental data. MIT recently published an article[3] about converting nanoindentation data into material properties with the help of a neural network, showing great potential in combining an analytical approach with the capacity of fine-tuning the system to understand experimental environments.

Authors: Ludvig Lindsjö & Fanny Linander
Written for: BorgWarner, CAE-Group Landskrona
Division of Production and Materials Engineering, Lund Faculty of Engineering

[1] Lindsjö & Linander: A method for developing stress-strain relationships using Nanoindentations, Lund, Dec. 2020.

[2] Baoxing Xu/Xi Chen: Determining engineering stress–strain curve directly from the load–depth curve of spherical indentation test, in: Journal of Materials Research 25.12 (2010), DOI: 10.1557/jmr.2010.0310, pp. 2297–2307.

[3] Lu et al.: Extraction of mechanical properties of materials through deep learning from instrumented indentation, in: Proceedings of the National Academy of Sciences 117.13 (2020), pp. 7052–7062, URL: https://www.pnas.org/content/117/13/7052.